Classical turning surfaces in solids: When do they occur, and what do they mean?

Aaron D. Kaplan*
Department of Physics, Temple University, Philadelphia, PA 19122

Stewart J. Clark
Centre for Materials Physics, Durham University, Durham, DH1 3LE, United Kingdom

Kieron Burke
Departments of Chemistry and Physics, University of California, Irvine, CA 92697

John P. Perdew
Departments of Physics and Chemistry, Temple University, Philadelphia, PA 19122

(Dated: July 28, 2020)

Classical turning surfaces of Kohn-Sham potentials, separating classically-allowed regions (CARs) from classically-forbidden regions (CFRs), provide a useful and rigorous approach to understanding many chemical properties of molecules. Here we calculate such surfaces for several paradigmatic solids. Our study of perfect crystals at equilibrium geometries suggests that CFRs are absent in metals, rare in covalent semiconductors, but common in ionic and molecular crystals. A CFR can appear at a monovacancy in a metal. In all materials, CFRs appear or grow as the internuclear distances are uniformly expanded. Calculations with several approximate density functionals and codes confirm these behaviors. A classical picture of conduction suggests that CARs should be connected in metals, and disconnected in wide-gap insulators. This classical picture is confirmed in the limits of extreme uniform compression of the internuclear distances, where all materials become metals without CFRs, and extreme expansion, where all materials become insulators with disconnected and widely-separated CARs around the atoms.

I. INTRODUCTION

The most basic property of an ordered solid is whether or not it is metallic [1–3]. The Sommerfeld free electron model of metallic conduction [4], which involves quantum mechanics only via a Fermi distribution of velocities, assumes a homogeneous system (uniform electron gas), but we wish to understand the effect of inhomogeneity. A simple classical picture of conduction is to consider an electron of energy ε in a single-particle effective potential, $v_{\rm eff}(\boldsymbol{r})$. If $\varepsilon > v_{\rm eff}(\boldsymbol{r})$ everywhere, this classical electron will move forever throughout the solid (or at least as far as its mean free path will allow), and the solid should be a metal. On the other hand, if the only classically allowed regions are disjoint regions bound to atoms, the solid should be strongly insulating. Unlike a classical electron, a quantum electron can tunnel into a classically-forbidden region.

The standard modern theory of conduction (for ordered solids) is that of Bloch bands, with insulators having filled bands below finite gaps in the spectrum [5]. At first glance, this appears to have little in common with the simple classical picture given above. But quantum theories derive from classical theories, and are connected to quantum mechanics via semiclassical approximations using classical trajectories. Consider what happens to a standard band structure as $\hbar \to 0$ keeping the Fermi energy fixed. For energies above the maximum of the potential everywhere, the bands become more free-electron like, as the inhomogeneity in the potential becomes less relevant. On the other hand, for energies below the maximum, the band becomes narrower and more localized as $\hbar$ shrinks. The importance of turning points to semiclassical (and density functional) approximations was prefigured in the cartoon of Fig. 1 of Ref. [6].

The Kohn-Sham (KS) potential [7] is the scalar potential that, acting on non-interacting electrons, yields a ground-state electron density equal to that of the real system. While not a physical observable, the KS potential is extremely useful as an interpretive tool. Inspired by earlier work that used the "potential acting on an electron in a molecule" (PAEM) [8, 9], Ospadov *et al.* [10] recently created a "periodic table of nonrelativistic classical turning radii" using the KS turning surface of the highest occupied KS orbital, defined as those points satisfying

$$v_s(\boldsymbol{r}) = \varepsilon_{\rm HO}, \tag{1}$$

where $v_s(\boldsymbol{r})$ is the KS potential, and $\varepsilon_{\rm HO}$ is the energy of the highest occupied orbital (the Fermi energy ε_F in a metal). They demonstrated that a classical turning surface could characterize bond types in molecules numerically and visually [10]. At equilibrium geometries, covalent bonds as in N_2 have fused (roughly ellipsoidal) turning surfaces, ionic bonds as in NaCl often have seamed surfaces, hydrogen bonds as in $(H_2O)_2$ have necked sur-

* kaplan@temple.edu

faces, and van der Waals bonds as in Ne_2 have bifurcated surfaces (with each part nearly spherical). The ratio of an equilibrium bond length to the sum of its atomic radii is roughly 0.5 for a covalent bond, 1.0 for an ionic or hydrogen bond, and 1.5 for a van der Waals bond. More recently, Gould *et al.* [11] found that the classical turning surface of H_2^+, which is approximately ellipsoidal at the equilibrium bond length, bifurcates when the bond length is stretched to about twice the turning radius of one dissociation product $H^{+0.5}$ (rigorously the same as the turning radius of a neutral hydrogen atom, ≈ 1.06 Å). Neutral atoms other than hydrogen typically have one or more electrons in the classically-forbidden region (CFR) outside their turning surfaces [12]. Earlier, Ref [13] had noted that a CFR emerges within the local density approximation (LDA) in stretched H_2 very near the Coulson-Fisher point, signaling the onset of strong correlation as the bond grows.

A turning surface in position space should not be confused with a Fermi surface in wavevector space. The turning surface defined here is the intersection in position-space of the KS potential with the Fermi level. If $\varepsilon_F > v_s(\boldsymbol{r})$ everywhere, there is no turning surface, whereas the Fermi surface is always well-defined. One could also define a turning surface in terms of the chemical potential $\mu \geq \varepsilon_F$ [14], which differs from $\varepsilon_{\rm HO}$ for non-metals, but using $\varepsilon_{\rm HO}$ in Eq. 1 is more practical and useful.

Here we present calculations of KS turning surfaces for a variety of simple solids. Our calculations are at the LDA and generalized gradient approximation (GGA) level of exchange-correlation approximations, which usually yield close approximations to more precise KS potentials in molecules (as both KS potential and $\varepsilon_{\rm HO}$ are typically too shallow by about the same amount). In Kohn-Sham density functional theory (KS DFT) [7], the KS potential $v_s(\boldsymbol{r})$ is a multiplicative operator. In generalized KS theory, the exchange-correlation potential of a meta-GGA or a hybrid functional (using the Hartree-Fock exchange energy) is a non-multiplicative operator, but can be replaced [15] by the local one needed to define a classical turning surface. One can apply all the concepts of Ref. [10] to analyze bonding in solids from a chemical viewpoint, but here we focus on the most elementary property of materials: are they metallic? In our classical conduction argument above, the effective potential is clearly the KS potential, and the most energetic electron is the highest-occupied level. If $\varepsilon_{\rm HO}$ is higher than the maximum value of the KS potential, there are no classical Fermi-energy turning surfaces and the system ought to be metallic. If not, and if $\varepsilon_{\rm HO}$ is so low that the classically-allowed regions are disconnected, the system ought to be insulating (with a wide gap). We expect semiconductors to lie somewhere in between these extremes.

This work discusses classical turning surface analogs and semiclassical interpretations of them for a variety of simple solids. Section II describes the computational tools used to extract and analyze the KS potential for metals, as presented in Section III, and band insulators presented in Section IV. Special attention is paid to the roles of strain and defects in forming CFRs within solids. Section V discusses how the CFR can be used to predict conduction properties. Section VI discusses the role of CFR connectedness in determining the conductive properties of solids. The Supplemental Materials section contains additional data.

To interpret our results correctly, we point out the following crucial points concerning gaps. It has long been known that the KS gap, i.e., the bandgap of the exact KS potential, does not match the true (fundamental charge) gap [14], and typically underestimates it. The KS gaps of strictly semilocal approximations like LDA or GGAs are typically close to the exact KS gap [16–18], and thus are often substantially less than the fundamental gap. Hybrid functionals and meta-GGAs yield larger gaps when treated in a generalized KS scheme [19]. When lattice parameters are stretched well beyond equilibrium, semilocal functionals may produce broken-symmetry solutions of lower energy, as is well-known in the paradigmatic case of stretched H_2 [20], but does not occur (at least for finite systems) with the exact functional. As all calculations in this paper use only semilocal functionals, they are in the KS scheme, yield gaps that are smaller than fundamental gaps, and can break symmetry.

II. COMPUTATIONAL METHODS

All ensuing calculations were performed with either the Vienna *ab initio* Simulation Package (VASP) [21], or the Castep code [22, 23], or both. All GGA calculations used the Perdew-Burke-Ernzerhof GGA [24], and all LSDA calculations used the Perdew-Zunger parameterization of the uniform electron gas correlation energy [25]. The calculations in VASP were performed with a cutoff energy of 800 eV, a Γ-centered mesh of spacing 0.08 $Å^{-1}$, energy convergence of 10^{-6} eV, and stress convergence at 10^{-3} eV/Å. To determine equilibrium geometries in VASP, for metals, first-order Methfessel-Paxton smearing with parameter of 0.2 was used, and for insulators, the Blöchl tetrahedron method was used. VASP's internal methods were used to determine the relaxed cell volume. In Castep, a density-mixing algorithm was used to reach self-consistency, and geometries were determined with a BFGS (Broyden-Fletcher-Goldfarb-Shanno) energy minimization scheme with the finite basis set corrected for stress [26]. After relaxation, a calculation at the equilibrium volume using the Blöchl tetrahedron method was performed to accurately determine the density of states. Accurate [27] PAW on-the-fly pseudopotentials were used throughout. Tables S6 to S54 (in the Supplemental Materials) present all raw data; machine readable data will be made available upon reasonable request.

For monolayers, a $45 \times 45 \times 1$ $\boldsymbol{k}$-point grid was used in conjunction with the Blöchl tetrahedron method. All

other parameters remain the same from bulk calculations. The c direction was padded with 30 Å of vacuum region to reduce interactions between image monolayers.

In density functional plane-wave codes, the densities and potentials are stored on a uniform grid $\boldsymbol{R}$, the dimensions of which are determined by the size of the unit cell and the plane-wave cutoff energy. Acceptable convergence of the total energy relies on suitable convergence of the potentials and densities on this grid. The values of $v_s(\boldsymbol{R})$ are obtained from this grid. In core regions, the true potential is much deeper than the pseudopotential, so these are classically allowed. Thus the PAW pseudopotential core regions were excluded from the CFR (frozen-core pseudopotentials were used in both VASP and Castep). The self-consistent electronic eigenstates give $\varepsilon_{\mathrm{HO}}$ (the Fermi energy ε_F in a metal), and the regions where $\varepsilon_{\mathrm{HO}} - v_s(\boldsymbol{R}) < 0$ define the CFR. We assign equal volume to each point relative to the primitive cell, as the real-space mesh is uniform. Suppose there are N_{prim} total real-space mesh points in the cell, and let the volume of the primitive cell be V_{prim}. Then the volume of any point is $V_{\mathrm{prim}}/N_{\mathrm{prim}}$. If there are N_{CFR} points at which $\varepsilon_{\mathrm{HO}} - v_s(\boldsymbol{r}) < 0$, the volume of the CFR is

$$V_{\mathrm{CFR}} = V_{\mathrm{prim}} N_{\mathrm{CFR}} / N_{\mathrm{prim}}. \tag{2}$$

The dimensionless, "fractional volume" of the CFR, which will be used in the ensuing figures and fits, is defined as

$$v \equiv V_{\mathrm{CFR}}/V_{\mathrm{prim}} = N_{\mathrm{CFR}}/N_{\mathrm{prim}}, \tag{3}$$

the number of real-space mesh points within the CFR relative to the total number of mesh points in the primitive cell.

As the fractional CFR volume $v \to 0$, our method requires ever finer real- and reciprocal-space meshes to resolve v. This need is limited by the resolution determined by the plane-wave cutoff energy. Our data for $v \ll 1$ will necessarily be more noisy than for larger values of v. Despite this, we show *a posteriori* that reasonable fits to $v(V_{\mathrm{prim}})$ may be found.

Each code uses differently-generated pseudopotentials with different optimal basis set cutoff energies (and hence pseudopotential grid sizes, etc.), different energy minimization schemes, and different Brillouin zone integration methods. To ensure that our method is not dependent upon the numerical methods of a particular code, we have verified that the Castep and VASP results are consistent.

III. OPENING CFRS IN METALS

As we see in Table I, no CFR is present in certain defect-free metals (Al, Cu, and Pt) at their equilibrium geometries. This is in line with our initial hunch, but does not extend to metals with monovacancies. A Pt supercell with a monovacancy defect harbors a small CFR; plotting this CFR in Fig. 1, we see that the classically-forbidden region encapsulates the center of the vacancy perfectly. Relaxation of the supercell volume was performed two ways: direct minimization of the stress tensor, and keeping the supercell volume fixed to the bulk volume while allowing ion positions to change.

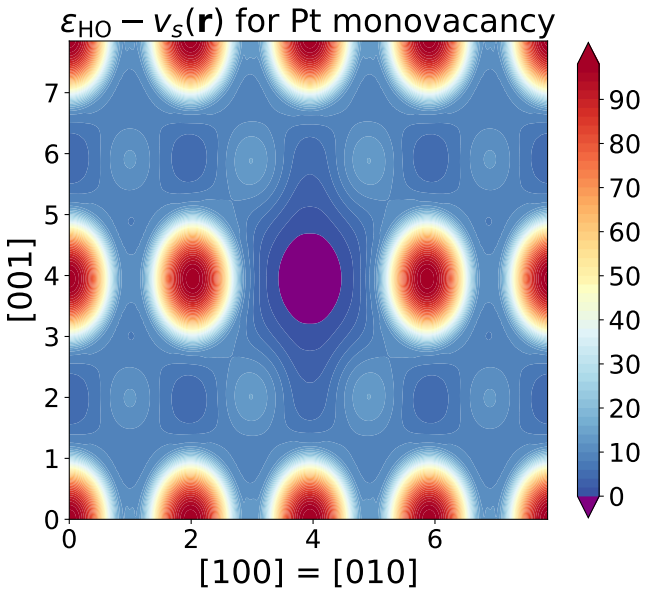

FIG. 1. A contour plot of $\varepsilon_{\mathrm{HO}} - v_s(\boldsymbol{r})$ as calculated with PBE along the [110] (conventional cubic indices) direction in the Pt monovacancy supercell. The CFR (purple) surrounds the defect, supporting the conjecture that the formation of a defect is accompanied by the formation of an internal curved surface. Regions within the PAW pseudopotential core radii are only included here to make the image clearer. For an analogous figure in Si, refer to S2 in the Supplemental Materials.

The vacancy defect formation energy can be recast as the energy needed to create a curved surface within a solid [28]. The localization of the CFR to the vacancy region is a clear manifestation of this. Carling *et al.* [29] found that the LDA is more accurate than GGAs for the Al monovacancy formation energy, in line with earlier results [30] for the jellium surface energy. They also found a very low electron density near the center of the vacancy, and large Friedel oscillations around it, consistent with a CFR near the center. Large voids and exterior surfaces would also give rise to extensive CFRs in any material.

The definition of the monovacancy volume given in Carling *et al.* differs from ours. Their method used the liquid drop model of jellium from Ref. [28] to extract the vacancy's volume from the vacancy defect formation energy. This method will generally yield larger volumes than the corresponding CFR volumes.

It is natural then to ask how far a metal needs to be stretched before a CFR emerges. In Fig. 2, we plot the fractional volumes of the LSDA and PBE CFRs as a function of the primitive cell volume. To find accurate

Solid (structure)	$\varepsilon_{\rm HO} - v_s^{\rm max}$ (eV)	CFR fraction	$V_{\rm prim}$ (Å^3)	Lattice Const. (Å)	Expt. Lattice Const. (Å)
Al (fcc)	5.75 (5.94)	0%	16.48 (15.81)	4.04 (3.98)	4.02 [31]
Cu (fcc)	5.56 (6.04)	0%	12.01 (10.94)	3.63 (3.52)	3.59 [31]
Pt (fcc, bulk)	4.76 (5.04)	0%	15.61 (14.90)	3.97 (3.90)	3.91 [32]
Pt monovacancy (fcc)	-1.18 (-1.00)	10.9% (5.2%)	15.39 (14.68)	3.95 (3.89)	3.91
	-1.29 (-1.29)	12.1% (6.4%)	15.61 (14.90)	3.97 (3.90)	

TABLE I. PBE and LSDA (parenthesized when different) values for the classically-forbidden regions (as a percentage of the total cell volume) and the relaxed primitive cell volumes and lattice constants in select metals. The percent volume is taken with respect to the primitive unit cell (percent volume per atom). For the first set of Pt monovacancy results, the cell volume and ion positions were relaxed; for the second set, the volume was fixed to the bulk value, and the ion positions were relaxed. Both sets of calculations used 31 ions in the supercell.

Solid (struc.)	DFA	c_0	c_1	c_2	c_3	R^2	V_c (Å^3)
Al (fcc)	LSDA	0.59	-1.32	0.90	-0.17	0.0008	48.08
		0.67	1.25	-7.22	5.96		71.18
	PBE	5.03	-17.31	20.16	-7.88	0.0011	54.68
		1.71	-8.48	22.46	-21.36		103.65
Cu (fcc)	LSDA	7.37	-24.41	27.18	-10.14	0.0002	29.69
		1.04	-1.47	2.31	-3.14		47.31
	PBE	12.97	-42.29	46.44	-17.12	0.0051	35.02
		1.25	-3.40	7.95	-7.35		51.29
Pt (fcc)	LSDA	7.37	-23.91	26.14	-9.60	0.0002	25.61
		1.01	-1.41	1.82	-2.30		39.01
	PBE	7.26	-23.32	25.35	-9.29	0.0027	26.78
		1.13	-2.71	6.17	-6.26		42.36
C (ds)	LSDA	1.01	-1.55	0.81	-0.27	0.0006	23.16
	PBE	1.02	-1.79	1.27	-0.50	0.0004	20.26
Ne (fcc)	LSDA	0.97	-0.27	-0.25	-0.44	0.0068	5.85
	PBE	1.02	-0.84	1.04	-1.22	0.0015	5.54
NaCl (rs)	LSDA	0.89	-0.23	-1.86	1.20	0.0002	30.70
	PBE	0.86	-0.09	-1.90	1.13	0.0002	28.88
Si (ds)	LSDA	0.92	-1.34	0.52	-0.10	0.0005	53.82
	PBE	0.96	-1.66	1.14	-0.44	0.0001	48.59
NiO (rs)	PBE	-0.14	4.45	-8.49	4.17	0.0004	29.56
		0.94	-0.68	-0.40	-0.07		48.29

TABLE II. Parameters for the fit functions presented in Figs. 2 and S4 (in the Supplemental Materials). The density functional approximation (DFA) column refers to either LSDA or PBE in VASP; for Castep fits, see Table S1 of the Supplemental Materials. The $\boldsymbol{c}$ parameters are dimensionless. R^2 is the sum of square residuals. V_c is the predicted critical primitive cell volume for onset of a CFR. For metals, the first (second) line gives the parameters $\boldsymbol{c}$ for $V_{\rm prim} < V_0$ ($\boldsymbol{d}$, for $V_{\rm prim} > V_0$, and V_0 is given in lieu of V_c). The fitted LSDA V_c for Ne is too large (i.e., it is larger than the smallest tabulated value of $V_{\rm prim}$ for which $v(V_{\rm prim}) > 0$); all other fitted values of V_c are within the correct bounds. Here, "ds" refers to diamond structure and "rs" to rock salt structure. NiO is treated as spin-unpolarized.

critical primitive cell volumes V_c for the emergence of a CFR, we perform a least squares fit to

$$v(V_{\rm prim}, \boldsymbol{c}) = \Theta(V_{\rm prim} - V_c) \sum_{m=0}^{3} c_m \left(\frac{V_c}{V_{\rm prim}} \right)^m \qquad (4)$$

where $V_{\rm prim}$ is the primitive cell volume, $0 \le v < 1$ is the fractional CFR volume, Θ is a step function, and the dimensionless $\boldsymbol{c} \equiv (c_0, c_1, c_2, c_3)$ are derived from least-squares fit parameters. Note that $\sum_{m=0}^{3} c_m = 0$, and $\partial v / \partial V_{\rm prim} > 0$ for $V_{\rm prim} - V_c = 0^+$. Fit parameters for PBE and LSDA data, as calculated in VASP, are listed in Table II. For the fit parameters of PBE data as calculated in Castep, refer to Table S1 in the Supplemental Materials.

Despite the possibility of noisy data at small CFR fractions, $0 < v \ll 1$, no lower cutoff on the VASP data was needed in the fitting process. The Castep data required a cutoff of $v_c = 0.01$ (for which any data with $v \le v_c$ was taken to have $v = 0$ instead), and a few elemental solids (Mg, Sr, Ba, Ra) required a higher cutoff, $v_c = 0.05$.

The form of Eq. 4 is selected because it makes v tend to zero as $V_{\rm prim}$ tends to V_c from above, and to a finite value (c_0) as $V_{\rm prim}$ tends to infinity. (A perfect fit over the whole range $V_{\rm prim} > V_c$, not needed here, would require $c_0 = 1$.) As the PAW core region is classically-allowed in an all-electron approach, there will always exist a classically-allowed region in this type of calculation. As our method has lower resolution for $v \ll 1$, we expect our fitted values of V_c to be estimates of the "true" values. V_c was determined by a root-finding algorithm. When possible, the value of V_c was constrained to lie between the largest tabulated value of $V_{\rm prim}$ for which $v = 0$, and the smallest tabulated value of $V_{\rm prim}$ for which $v > 0$. When that was not possible, a tolerance of 3% was afforded, which we note in Table II as well.

Many of the metals presented here exhibit more complex $V_{\rm prim}$-dependence than the insulators, so we perform a piecewise fit

$$v_{\rm metal}(V_{\rm prim}) = v(V_{\rm prim}, \boldsymbol{c})\Theta(V_0 - V_{\rm prim}) + v(V_{\rm prim}, \boldsymbol{d})\Theta(V_{\rm prim} - V_0), \qquad (5)$$

where both functions on the RHS are of the form of Eq. 4. To perform the fit, we chose a value of V_0 to model the point of inflection of the curve, and the fitting procedure detailed above was followed for $V_{\rm prim} \le V_0$. We then required that $v(V_{\rm prim})$ and $\partial v(V_{\rm prim})/\partial V_{\rm prim}$ be continuous at $V_{\rm prim} = V_0$, fixing d_0 and d_1. A least squares fit was then performed to yield d_2 and d_3. V_0 was modulated to minimize the sum of square residuals, $R^2 = \sum_{V_{\rm prim}} |v^{\rm approx}(V_{\rm prim}) - v(V_{\rm prim})|^2$. To prevent over-fitting, the lowest value of V_0 for which $R^2 < 10^{-3}$

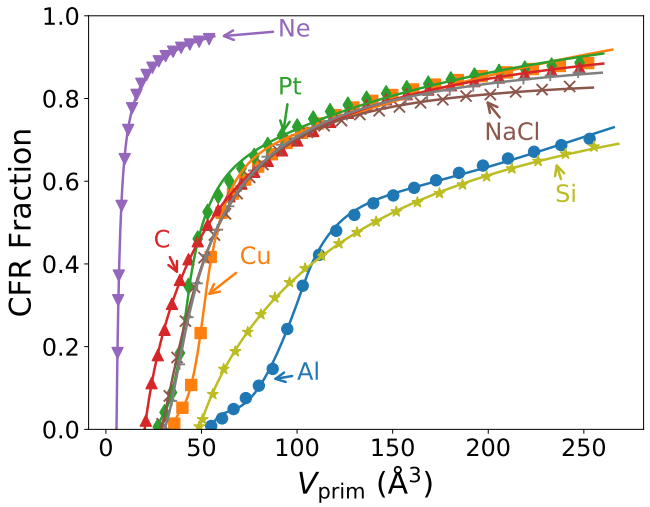

FIG. 2. Emergence of PBE CFRs in Al (blue closed circles), Cu (yellow squares), Pt (green diamonds), C (red point-up triangles), Ne (purple point-down triangles), NaCl (brown crosses), and Si (olive stars) as a function of the primitive cell volume. All lines are fits given in Table II. As Al, Cu, C and Si have no CFR at their relaxed lattice parameters, each lattice must be stretched to introduce a CFR. Conversely, Ne and NaCl must be compressed to eliminate their CFRs; for completeness, the full NaCl curve is presented here. The curve for spin-unpolarized NiO is almost identical to that of NaCl (see Fig. S3 of the Supplemental Materials). The LSDA curves are very similar, see Fig. S4 in the Supplemental Materials. For PBE curves as calculated in Castep, see Fig. S5 in the Supplemental Materials.

was deemed the optimal fit.

Let a be the equilibrium lattice parameter for a given solid as given by Table I. From the critical lattice parameters in Table II, we see that a CFR opens in Cu at a lattice parameter of $1.43a$ for PBE (about 2.9 times the equilibrium volume). The CFR appears before the KS gap opens. The fits predict that a CFR in Al opens at $1.49a$ for PBE (about 3.3 times the equilibrium volume), also without a KS band gap opening. For Pt, the CFR opens at $1.20a$ (about 1.7 times the equilibrium volume), without a gap opening. By bandgap, we always mean the gap determined from our approximate band structure or density of states, rather than the fundamental gap.

Note also that the LSDA and PBE curves in Figs. 2 and S4 for Al, Cu, and NaCl cross, whereas those for elemental insulators do not. For the elemental insulators, the difference between the LSDA and PBE curves is always of the same sign.

IV. CFRS IN INSULATORS

The situation for insulators, as shown in Table III, is more nuanced, and there are clear variations in the volumes of approximate CFRs found from different approximate exchange-correlation functionals. Our intuition that the presence of a CFR is accompanied by the opening of a band gap is not borne out.

However in weakly interacting and van der Waals solids, like graphite and Ne, there are noticeable PBE CFRs. The small (1%) PBE CFR volume in graphite (hexagonal C) at its experimental lattice constants reflects the semimetallic nature of this material. The PBE CFR in graphite lies between monolayers, just as one might expect for few-layer graphene. The CFR volume is nearly 20% of the PBE equilibrium cell volume in graphite because PBE underestimates intermediate-range van der Waals interactions, and thus overestimates the equilibrium spacing. This fraction is reduced to 1% when the experimental cell volume is used instead. The LSDA finds no CFR in graphite, which may be related to the LSDA's underestimation of equilibrium lattice constants. For the prototypical semiconducting layered material MoS_2, we see the same pattern. The LSDA underestimates the equilibrium c lattice parameter, yielding no CFR. PBE dramatically overestimates the c parameter, yielding a CFR encompassing 22.3% of the primitive cell volume. Note that the LSDA and PBE are similarly accurate for the sandwich-layer thickness z (the distance between neighboring layers of sulfur atoms).

Consider instead a monolayer of graphite or MoS_2. For these sheets, we use the bulk a and z lattice parameters found by relaxing the equilibrium cell volume. We find no CFR within the monolayer region for graphene or monolayer MoS_2 using both the LSDA and PBE. Thus, no in-plane CFR is present in graphene, and no in-sandwich CFR is found in monolayer MoS_2.

Crystalline NaCl, just like its molecular form [10], also has large PBE and LSDA CFRs. Because NaCl is a prototypical ionic solid, we expect that many other ionic crystals and more weakly-bound crystals at equilibrium will exhibit CFRs.

Referring back to Table. II, we see that a CFR emerges in ds C when the lattice is stretched to $1.21a$ for PBE (about 1.8 times the equilibrium volume); for ds Si, a CFR is predicted to emerge at $1.06a$ for PBE (about 1.2 times the equilibrium volume). Thus it appears that PBE predicts the emergence of a CFR in an insulator when the lattice is stretched not much further past its equilibrium point. For both Si and C, the band gap is substantial even when the CFR begins to emerge.

The classical radius of the free Ne atom is 0.87 Å, in both PBE [39], and with a more accurate Kohn-Sham potential [10], with a volume of 2.76 Å^3. The experimental lattice constant is 4.464 Å [35], corresponding to a cell volume per atom of 22.24 Å^3. The CFR predicted by Ref. [10] is then $(22.24 - 2.76)/22.24 \approx 88\%$ of the total cell volume, agreeing with the values in Table III. A Ne atom in solid Ne at the equilibrium lattice constant is very similar to a free Ne atom.

In the same vein as for C and Si, we can compress the Ne lattice until the CFR vanishes, as seen in Fig. 2. The Ne CFR is predicted to vanish at $0.62a$ for PBE. One

Solid (structure)		$\varepsilon_{\rm HO} - v_s^{\rm max}$ (eV)	CFR fraction	$V_{\rm prim}$ (Å^3)	Lattice Const(s). (Å)	Expt. Lattice Const(s). (Å)
Si (ds)		0.91 (1.44)	0%	40.89 (39.43)	5.47 (5.40)	5.42 [31]
C (ds)		5.59 (6.62)	0%	11.40 (11.04)	3.57 (3.53)	3.55 [31]
C (hex)	relaxed	-3.06 (1.04)	18.5% (0%)	42.80 (34.45)	2.47 (2.45) (a), 8.12 (6.65) (c)	2.46 (a), 6.71 (c) [33, 34]
	expt.	-0.28 (0.92)	1.0% (0%)	35.25	2.46 (a), 6.71 (c)	2.46 (a), 6.71 (c)
Ne (fcc)	relaxed	-14.44 (-9.23)	87.1% (78.1%)	23.67 (14.39)	4.56 (3.86)	4.46 [35]
	expt.	-14.20 (-10.90)	86.3% (86.3%)	22.24	4.46	4.46
NaCl (rs)	relaxed	-3.38 (-2.05)	34.6% (17.7%)	46.23 (40.90)	5.70 (5.47)	5.57 [31]
	expt.	-3.06 (-2.30)	29.6% (22.4%)	43.18	5.57	5.57
MoS_2 (P6/mmc or $2H_b$)		-4.24 (0.01)	22.3% (0%)	128.46 (101.94)	3.18 (3.12) (a), 14.62 (12.07) (c), 3.12 (3.11) (z)	3.16 (a), 12.29 (c), 3.17 (z) [36]
NiO (rs)		4.97	0%	18.01	4.16	4.17 [37]

TABLE III. PBE and LSDA (parenthesized when different) values for the classically-forbidden regions, primitive cell volumes, and lattice constants of select insulators. For graphite, Ne, and NaCl, two sets of results are shown: the first at a relaxed PBE geometry, and the second at the experimental equilibrium geometry. The percent volume is taken with respect to the primitive cell (percent volume per atom). Here, "ds" refers to diamond structure, "hex" to simple hexagonal structure (with a four-point basis for graphite), and "rs" to rock salt structure. The layered structure of MoS_2 is itself a prototype for dichalcogenide structure, and is often referred to as the "MoS_2 structure," or by its polytype $2H_b$ [36], or by its point group P6/mmc [38]. The a and c parameters have the same meaning as in a simple hexagonal lattice, the z parameter (sometimes called $2z$) is the spacing between neighboring sulfur layers. No LSDA calculation was performed for spin-unpolarized NiO.

might expect the bandgap to shrink as the CFR collapses, but the *opposite* is true. For the smallest lattice constant calculated here (2.85 Å), the band gap is roughly 18.57 eV, compared to a gap of about 11.51 eV (11.45 eV) at the PBE equilibrium (experimental) lattice constant, consistent with previous work that used PBE to study phases of Ne under pressure [40]. Intuition suggests that the Ne CFR should not be fully suppressed before the classical turning surfaces between adjacent atoms just touch, at a nearest-neighbor separation of $2(0.87) = 1.74$ Å, using the result from Ref. [10]. This is substantially smaller than the nearest-neighbor spacing in crystalline Ne for which the PBE CFR is wiped out, $2.81/\sqrt{2} \approx 2.00$ Å. Thus, unexpectedly, the critical lattice constant in Ne makes the nearest-neighbor distance noticeably greater than twice the turning radius of the free atom.

As the lattice is compressed, two competing effects determine the bandgap: the bands widen, reducing the gap; and the center of the conduction band is shifted upwards with respect to the center of the valence band, widening the gap. (For an example, see the silicon density of states at equilibrium and at a mild expansion, in Fig. S1 of the Supplementary Material.) This leads to a non-trivial (non-monotonic) dependence of the gap upon the lattice parameter.

V. PERIODIC TRENDS

To get an overall sense of how well (or poorly) the classical turning surface yields information on conduction, Fig. 3 demonstrates one way to classify this, by plotting the fitted values of V_c against the equilibrium $V_{\rm prim}$ for various solids. The elemental solids beyond those emphasized in the main text are in Groups 1 (alkali metals), 2 (alkaline earth metals), 14 (Group IV, carbon group) and 18 (rare, inert, or noble gases). The parameters of the fit functions (Tables S2-S5), as well as full strain curves for these solids (Figs. S6-S9) can be found in the Supplementary Materials. The figure shows that the existence of a CFR at equilibrium comes close to classifying a solid as an insulator or metal. No metal has an equilibrium CFR, but some insulators need a small expansion to produce one.

Moreover, we can see very clear trends in the strain curves of elemental solids as one goes down a column of the periodic table. In Fig. 4(a), we plot the strain curves as a function of $V_{\rm prim}/V_c$, for elemental insulators. The noble gases all fall on one line, except for the lightest, He, while the carbon group elements fall on another, except for the lightest, C. Clearly, each group has its own characteristic curve, which differs from one group to another.

The alkali and alkali-earth metals show similar, but more complex behavior, as shown in Fig. 4(b). The green line is for the heavier alkalis, and the orange line is for the alkali-earths. Now the lighter two alkalis, Li and Na, are shown in blue, and clearly share a shape that is distinct from the later alkalis. They follow the alkali earth curve closely, except for a dip around $1.4V_c$. Moreover, Mg (in gray) is the odd one out of the alkali earths, rather than Be. For small strains, Mg behaves like all other alkali earths, but when greatly expanded, behaves more like an alkali.

Naturally, within a column of the periodic table, the critical CFR volume V_c increases with atomic number, as shown in the Supplementary Materials. If we define

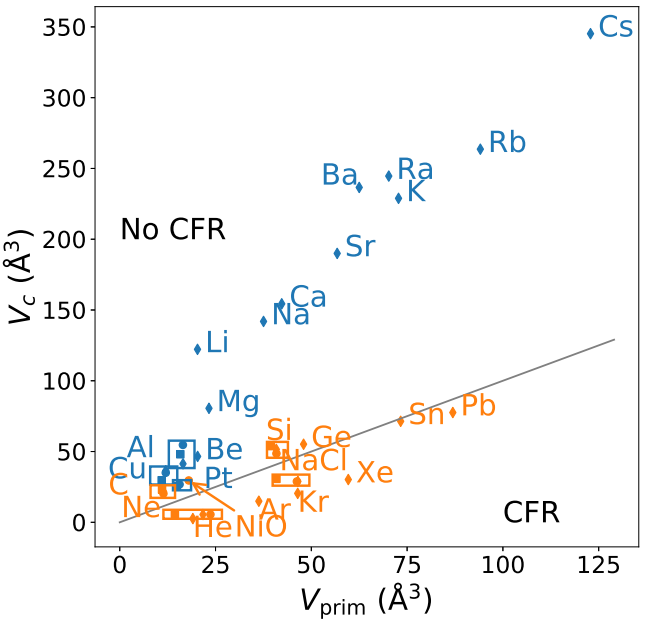

FIG. 3. Contrasting the amount of strain needed to induce a CFR for various solids. The grey line is $V_{\rm prim} = V_c$, so that solids lying above the grey line have no CFR at equilibrium, and solids below the line have a CFR at equilibrium. For the VASP data (circles for PBE and squares for LSDA), $V_{\rm prim}$ is the equilibrium cell volume. For the Castep data (diamonds all with PBE), $V_{\rm prim}$ is the equilibrium cell volume except for the rare gases, for which $V_{\rm prim}$ takes the experimental value. Metals are shown in blue, and insulators in orange. Note that Sn and Pb were calculated in the cubic diamond structure (α- or grey Sn), which are likely non-metallic phases. In particular, grey Sn has a 0.1 eV gap [5]. NiO is treated as spin-unpolarized.

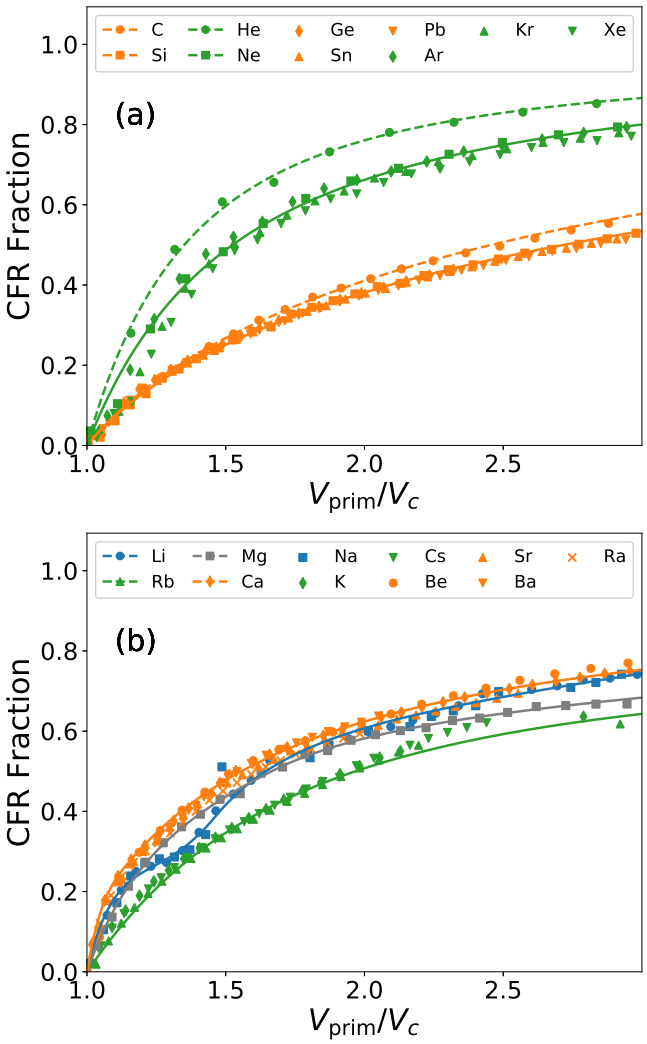

FIG. 4. Trends among groups of elements emerge when plotting the CFR fraction against the dimensionless $V_{\rm prim}/V_c$, where V_c is fitted. All data shown here was calculated with PBE in Castep. Panel (a) is for the metals, and panel (b) for the insulators.

the volume of a free atom as $V_{\rm at} = 4\pi r_{\rm TS}^2/3$, where $r_{\rm TS}$ is the radius of the atom's classical turning surface from Ref. [10], then the ratio $V_c/V_{\rm at}$ is of order 1 and seems to approach a column-dependent large-Z limit (with Z the nuclear charge, see Tables S2-S5). The first ionization energies of the atoms exhibit similar behavior [41].

VI. CFR CONNECTEDNESS

In the introduction, we described a (semi-) classical model of solids that defined metals and insulators by their turning surface properties. In this model, a metal would have a connected classically-allowed region (CAR), and an insulator would have a disconnected CAR.

In Figure 5, we plot the evolution of the CFR and CAR in Si using PBE as a function of the lattice parameter. At equilibrium (panel (a)), there is no CFR. Just above V_c (panel (b)), the CAR is clearly connected and the CFR is disconnected. As the lattice is stretched further (panel (c)), the CFR grows and connects. Under an even more extreme strain (panel (d)), the CFR dominates the primitive cell, but the CAR remains connected, albeit not simply. The bandgap increases from 0.55 eV at $a = 5.47$ Å to 0.81 eV at $a = 5.80$ Å, then decreases to 0.71 eV at $a = 5.87$ Å before rapidly falling toward zero. In Fig. 6, we show a three-dimensional view of the Si turning surface at $a = 7.11$ Å. Both the CFR and CAR are simultaneously fully connected. The geometry of Fig. 6 is very nearly identical to that of Fig. 5(c). To generate the plane of Fig. 5(c) from Fig. 6, one would make a diagonal cut from the front bottom left corner to the rear upper right corner of the cell in Fig. 6.

In the limit of extreme expansion, the CAR's are always disconnected and well-separated. Electron tunneling is inhibited through energy barriers that are wide or high. The bands will narrow to atomic levels. For a solid built from closed-shell atoms like Ne, the bandgap will tend to a non-zero and typically large value, while for a

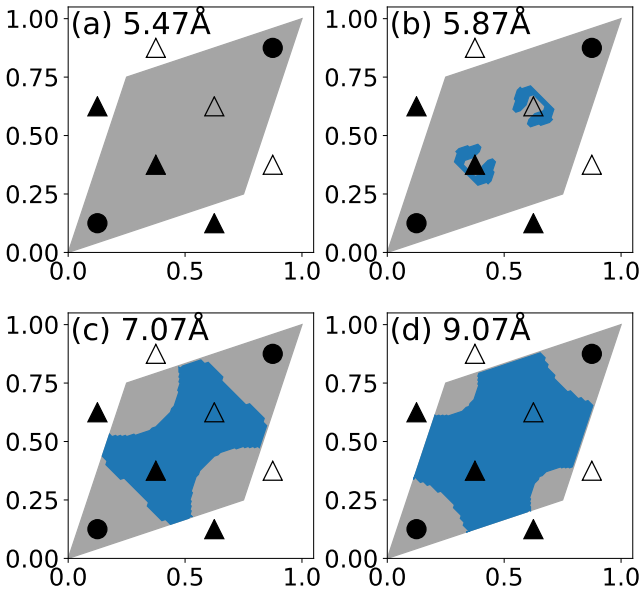

FIG. 5. Evolution of the PBE CAR (grey) and CFR (blue) in ds Si as a function of the lattice parameter a plotted along the plane $z = (x + y)/2$ (i.e., the plane containing the line joining the origin and the point (a, a, a)) within the primitive cell. Ions located in plane are labelled with a black circle, those above with a black triangle, and those below with an open triangle. The lattice constant a is 5.47 Å in (a), 5.87 Å in (b), 7.07 Å in (c), and 9.07 Å in (d).

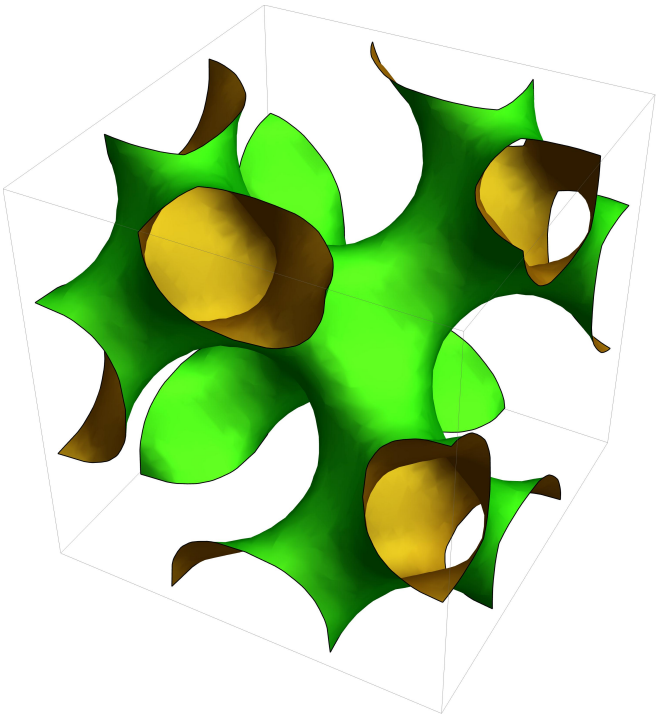

FIG. 6. The surface shows the CAR (outside, green) and CFR (inside, yellow) for silicon at $1.30a$. Both regions are simultaneously fully connected.

solid built up from open-subshell atoms like silicon, the bandgap will tend to a zero or small value (depending on whether the Kohn-Sham potential of the free atom is constrained to the symmetry of its external potential).

As the lattice is put under extreme expansive strain, we expect all solids to eventually transition to an insulating state, with disconnected and well-separated CAR's. In this limit, the bandgap can become large, small, or zero. If the lattice is compressed well below the equilibrium geometry, we expect any solid to eventually transition to a metallic state, with zero bandgap and a connected CAR.

VII. CONCLUSIONS

For the solids studied here, our calculations found no CFRs for metals, large CFRs for wide-gap insulators, and the emergence of CFRs when small-gap semiconductors are mildly expanded. Since standard density-gradient expansions are derived for slowly-varying densities without CFRs, the absence of CFRs in metals at equilibrium suggests that generalized gradient approximations (like or beyond PBE) should work especially well for them.

A monovacancy in a metal can induce a CFR, and an expansive strain in any material can induce a CFR or increase its volume. Moreover, the emergence of a CFR does not necessarily accompany the opening or closing of a band gap.

The volume of a CFR is a function of the lattice strain. Both metals and band insulators without a CFR at their equilibrium geometry can be stretched to introduce a CFR. Those wider-gap insulators with a CFR at equilibrium can be compressed until the CFR vanishes. Layered materials may have a CFR at equilibrium if a density functional approximation tends to stretch the c lattice parameter, as PBE does.

CFRs are also characteristic of perfect ionic and molecular crystals at equilibrium. Our analysis supports the conclusion that rare gas atoms in the crystalline phase are nearly free. Ionic crystals have large CFRs. We showed that graphite and MoS_2, where intermediate-range van der Waals interactions dominate between monolayers, have CFRs located solely between monolayers, and that their corresponding monolayers have no in-plane CFR. Our work demonstrates that weakly-bound solids tend to have prominent CFRs. Hydrogen-bonded crystals like ice, while not tested here, can be expected to have substantial CFR volume fractions, as suggested by Fig. 8 for the water dimer in Ref. [10].

The connectedness of a CFR seems to play a role in a system's conductivity. It was shown that the CFR in Si near the critical volume V_c is disconnected. As the lattice is stretched further, the CFR grows, eventually subsuming much of the primitive cell. The Si bandgap closes very nearly at the same V_{prim} that the CFR connects, indicating a semiclassical insulator-metal transi-

tion. A semiclassical picture suggests that a connected CAR and zero bandgap indicate a metallic state, found under extreme compression for any solid. As a corollary, disconnected and well-separated CAR's indicate an insulating state, and are found under strong expansion of the lattice.

Interacting quantum mechanical electrons can insulate through the Mott mechanism. We looked for CFRs in zero-gap spin-unpolarized NiO, a paradigm Mott insulator, but did not find one at the equilibrium lattice constant a. A CFR appeared at a lattice constant $1.18a$ (see Tables II and III). Our PBE calculations for NiO at equilibrium confirmed that a gap appears when the spin symmetry is allowed to break to antiferromagnetic order.

This is the first work to attempt to classify CFRs in solids, and without doubt more inquiry is needed to determine if CFRs are hallmarks of other phenomena in solids.

ACKNOWLEDGMENTS

ADK acknowledges the support of the Department of Energy (DOE), Basic Energy Sciences, under grant No. de-sc0012575. SJC acknowledges Engineering and Physical Sciences Research Council support on grant EP/P022782/1. KB was supported by DOE under grant no. DE-FG02-08ER46496. JPP acknowledges the support of the National Science Foundation under grant number DMR-1939528.

[1] N. F. Mott and R. H. Fowler, Proc. Roy. Soc. A **153**, 699 (1936).
[2] W. Kohn, Phys. Rev. **133**, A171 (1964).
[3] W. Kohn, Metals and insulators, in Many-body Physics, edited by C. DeWitt and R. Balian (Gordon and Breach, New York, 1968) pp. 353–411.
[4] A. Sommerfeld and N. H. Frank, Rev. Mod. Phys. **3**, 1 (1931).
[5] N. W. Ashcroft and N. D. Mermin, Solid State Physics (Holt, Rinehart and Winston, 1976).
[6] P. Elliott, D. Lee, A. Cangi, and K. Burke, Phys. Rev. Lett. **100**, 256406 (2008).
[7] W. Kohn and L. J. Sham, Phys. Rev. **140**, A1133 (1965).
[8] Z.-Z. Yang and E. R. Davidson, Int. J. Quantum Chem. **62**, 47 (1997).
[9] Z.-Z. Yang and D.-X. Zhao, Chem. Phys. Lett. **292**, 387 (1998).
[10] E. Ospadov, J. Tao, V. N. Staroverov, and J. P. Perdew, Proc. Nat. Acad. Sci. U.S.A. **115**, E11578 (2018).
[11] T. Gould, B. T. Liberles, and J. P. Perdew, J. Chem. Phys. **152**, 054105 (2020).
[12] S. Schwalbe, L. Fiedler, K. Trepte, J. Kortus, S. Lehtola, and J. P. Perdew, work in progress.
[13] K. Burke, A. Cancio, T. Gould, and S. Pittalis, J. Chem. Phys. **145**, 054112 (2016).
[14] J. P. Perdew, R. G. Parr, M. Levy, and J. L. Balduz Jr., Phys. Rev. Lett. **49**, 1691 (1982).
[15] E. Ospadov, I. G. Ryabinkin, and V. N. Staroverov, J. Chem. Phys. **146**, 084103 (2017).
[16] J. P. Perdew, What do the Kohn–Sham orbital energies mean? how do atoms dissociate?, in Density Functional Methods in Physics, edited by R. M. Dreizler and J. da Providencia (Plenum, New York, 1985) p. 265.
[17] J. P. Perdew, Int. J. Quant. Chem. Symp. **19**, 497 (1986).
[18] A. M. M. Grüning and A. Rubio, J. Chem. Phys. **124**, 154108 (2006).
[19] J. P. Perdew, W. Yang, K. Burke, Z. Yang, E. K. Gross, M. Scheffler, G. E. Scuseria, T. M. Henderson, I. Y. Zhang, A. Ruzsinszky, H. Peng, J. Sun, E. Trushin, and A. Görling, Proc. Nat. Acad. Sci. U.S.A. **114**, 2801 (2017).
[20] J. P. Perdew, A. Savin, and K. Burke, Phys. Rev. A **51**, 4531 (1995).
[21] G. Kresse and J. Hafner, Phys. Rev. B **47**, 558 (1993); Phys. Rev. B **49**, 14251 (1994); G. Kresse and J. Furthmüller, Phys. Rev. B **54**, 11169 (1996); Comp. Mater. Sci. **6**, 15 (1996).
[22] M. D. Segall, P. J. D. Lindan, M. J. Probert, C. J. Pickard, P. J. Hasnip, S. J. Clark, and M. C. Payne, J. Phys. Condens. Matter **14**, 2717 (2002).
[23] S. J. Clark, M. D. Segall, C. J. Pickard, C. J. Hasnip, M. J. Probert, K. Refson, and M. C. Payne, Z. Fur Kryst. **220**, 567 (2005).
[24] J. P. Perdew, K. Burke, and M. Ernzerhof, Phys. Rev. Lett. **77**, 3865 (1996).
[25] J. P. Perdew and A. Zunger, Phys. Rev. B **23**, 5048 (1981).
[26] G. P. Francis and M. C. Payne, J. Phys. Condens. Matter **2**, 4395 (1990).
[27] K. Lejaeghere, G. Bihlmayer, T. Björkman, P. Blaha, S. Blügel, V. Blum, D. Caliste, I. E. Castelli, S. J. Clark, A. Dal Corso, S. De Gironcoli, T. Deutsch, J. K. Dewhurst, I. Di Marco, C. Draxl, M. Dułak, O. Eriksson, J. A. Flores-Livas, K. F. Garrity, L. Genovese, P. Giannozzi, M. Giantomassi, S. Goedecker, X. Gonze, O. Grånäs, E. K. Gross, A. Gulans, F. Gygi, D. R. Hamann, P. J. Hasnip, N. A. Holzwarth, D. Iuan, D. B. Jochym, F. Jollet, D. Jones, G. Kresse, K. Koepernik, E. Küçükbenli, Y. O. Kvashnin, I. L. Locht, S. Lubeck, M. Marsman, N. Marzari, U. Nitzsche, L. Nordström, T. Ozaki, L. Paulatto, C. J. Pickard, W. Poelmans, M. I. Probert, K. Refson, M. Richter, G. M. Rignanese, S. Saha, M. Scheffler, M. Schlipf, K. Schwarz, S. Sharma, F. Tavazza, P. Thunström, A. Tkatchenko, M. Torrent, D. Vanderbilt, M. J. Van Setten, V. Van Speybroeck, J. M. Wills, J. R. Yates, G. X. Zhang, and S. Cottenier, Science **351**, 10.1126/science.aad3000 (2016).
[28] J. P. Perdew, Y. Wang, and E. Engel, Phys. Rev. Lett. **66**, 508 (1991).
[29] K. Carling, G. Wahnström, T. R. Mattsson, A. Mattsson, N. Sandberg, and G. Grimvall, Phys. Rev. Lett. **85**, 3862 (2000).
[30] L. A. Constantin, J. M. Pitarke, J. F. Dobson, A. Garcia-

Lekue, and J. P. Perdew, Phys. Rev. Lett. **100**, 036401 (2008), and earlier references within.
[31] J. Sun, M. Marsman, G. Csonka, A. Ruzsinszky, P. Hao, Y.-S. Kim, G. Kresse, and J. P. Perdew, Phys. Rev. B **84**, 035117 (2011).
[32] P. Haas, F. Tran, and P. Blaha, Phys. Rev. B **79**, 085104 (2009).
[33] Y. X. Zhao and I. L. Spain, Phys. Rev. B **40**, 993 (1989).
[34] P. Trucano and R. Chen, Nature **258**, 136 (1975).
[35] P. Schwerdtfeger and A. Hermann, Phys. Rev. B **80**, 064106 (2009).
[36] T. Böker, R. Severin, A. Müller, C. Janowitz, R. Manzke, D. Voß, P. Krüger, A. Mazur, and J. Pollmann, Phys. Rev. B **64**, 23505 (2001).
[37] F. Tran, P. Blaha, K. Schwarz, and P. Novák, Phys. Rev. B **74**, 1 (2006).
[38] M. Kan, J. Y. Wang, X. W. Li, S. H. Zhang, Y. W. Li, Y. Kawazoe, Q. Sun, and P. Jena, J. Phys. Chem. **118**, 1515 (2014).
[39] E. Ospadov, V. N. Staroverov, and J. P. Perdew, work in progress.
[40] Y.-g. He, X.-z. Tang, and Y.-k. Pu, Physica B **405**, 4335 (2010).
[41] L. A. Constantin, J. C. Snyder, J. P. Perdew, and K. Burke, J. Chem. Phys. **133**, 241103 (2010).

SUPPLEMENTAL MATERIALS FOR "CLASSICAL TURNING SURFACES IN SOLIDS: WHEN DO THEY OCCUR, AND WHAT DO THEY MEAN?"

Here we include extra figures, fit parameters, and data tables that may prove useful for future work. A figure of the density of states for Si at its PBE equilibrium geometry, and at the critical lattice parameter, is given in Fig. S1. A contour plot of $\varepsilon_{\mathrm{HO}} - v_s(\boldsymbol{r})$ in Si along the same plane as in Fig. 1 of the main text is included in Fig. S2.

Fig. S3 is analogous to Fig. 2 of the main text, but emphasizes the shapes of the strain-CFR curves by plotting V_{prim}/V_c. A plot of the LSDA fractional CFR volumes in the same manner as Fig. 2 in the main text, with PBE curves superposed faintly, is included in Fig. S4. Table S1 enumerates fitted critical volumes V_c for a comparison between VASP and Castep.

Last are a series of figures and tables for showing fitted strain curves for select main group elements as calculated with PBE in Castep, and using the fitting procedure in the main text, plotted separately for the Group 1, Group 2, Group 14, and Group 18 elemental solids.

We also include numerous tables (Tables S6-S54) enumerating the raw data used for fitting and generating figures. All data presented is available in this text, and machine-readable data will be made available at reasonable request.

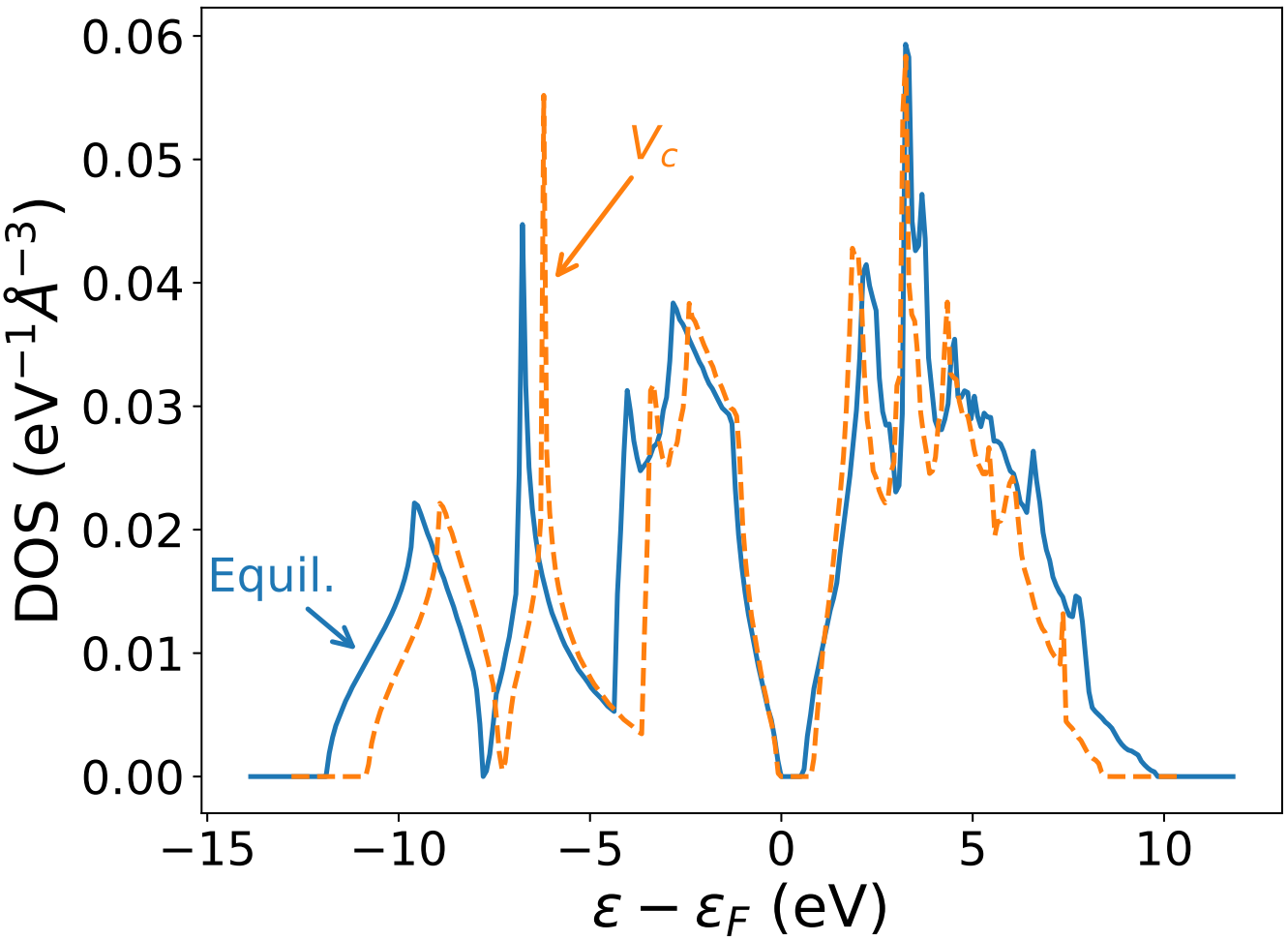

FIG. S1. Intensive density of states plots for Si at both the PBE equilibrium lattice parameter 5.47 Å (blue), and at the critical lattice parameter 5.81 Å (orange).

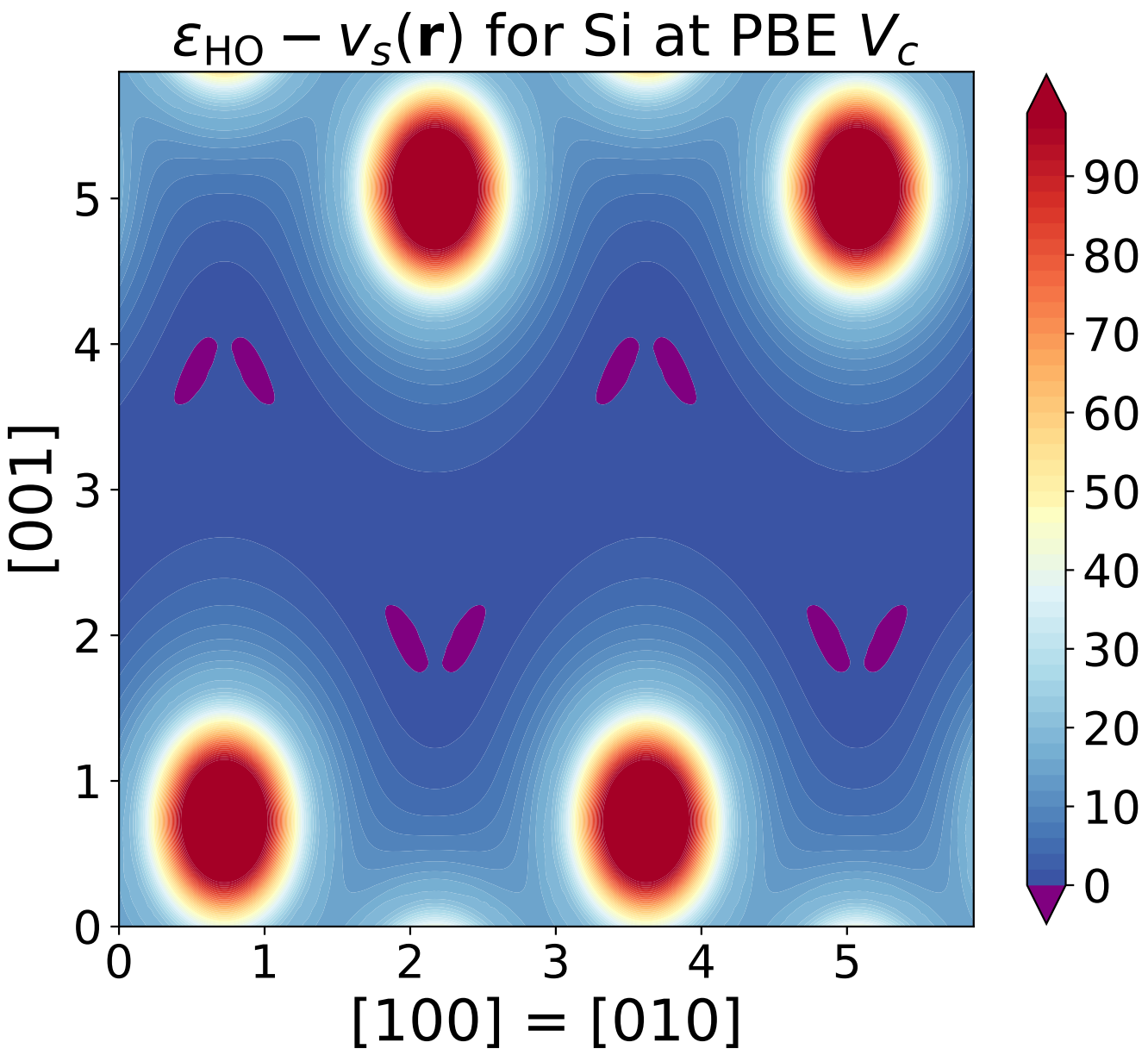

FIG. S2. Contour plot of Si along the [110] (conventional cubic indices) direction at the PBE critical lattice constant $a_c = 5.79$ Å, analogous to Fig. 1 in the main text. The CFR (purple) is minute at this volume, about 0.53% of the primitive cell volume, and located in the interstice. While this indicates the fit is not perfect, it provides a reasonable upper bound to a_c.

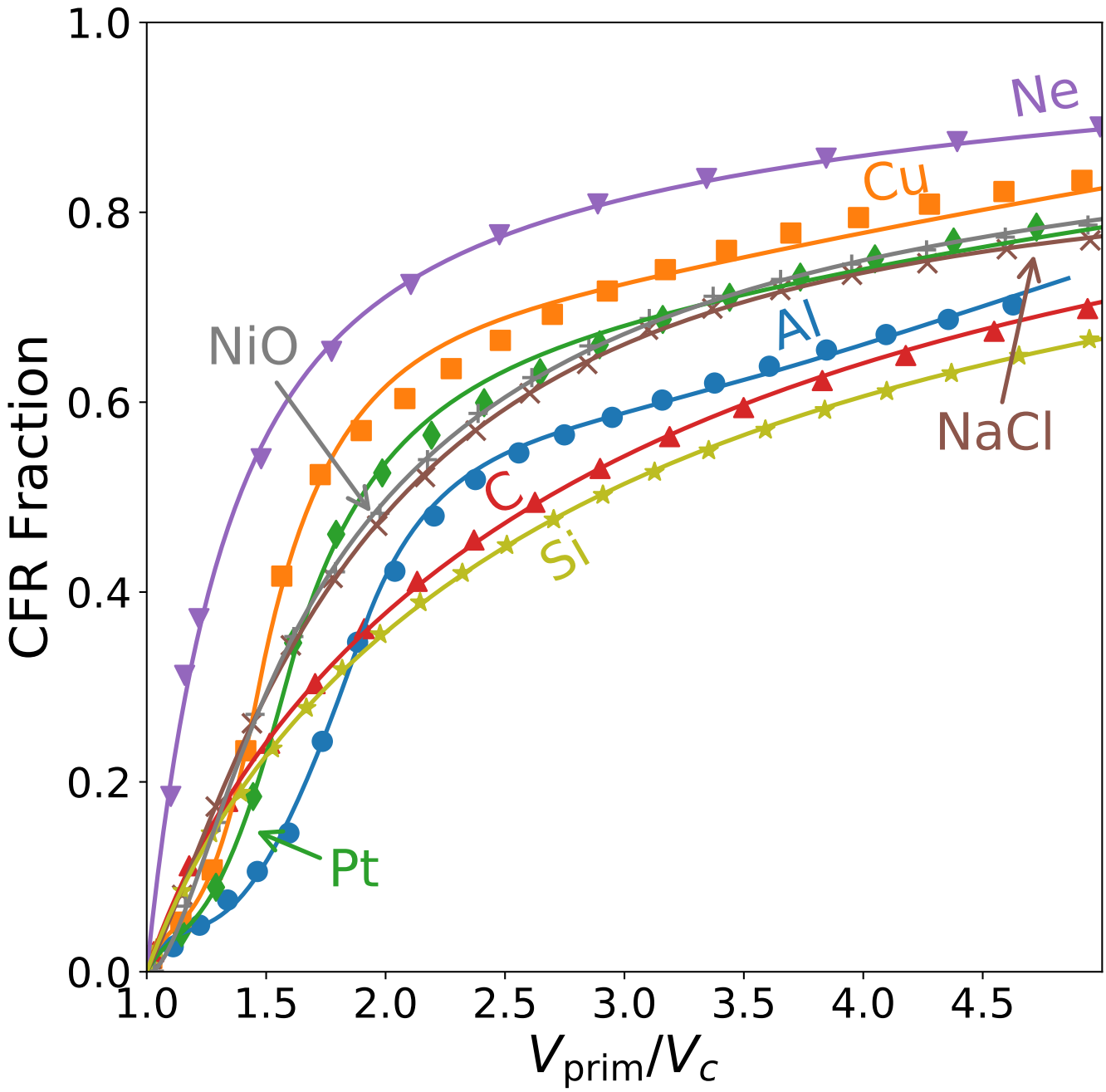

FIG. S3. Figure analogous to Fig. 2 in the main text, but plotting V_{prim}/V_c to emphasize the shapes of the strain-CFR curves. Perhaps expectedly, the C and Si curves have exceedingly similar shapes. Quite unexpectedly, the NaCl and spin-unpolarized NiO curves are nearly identical.

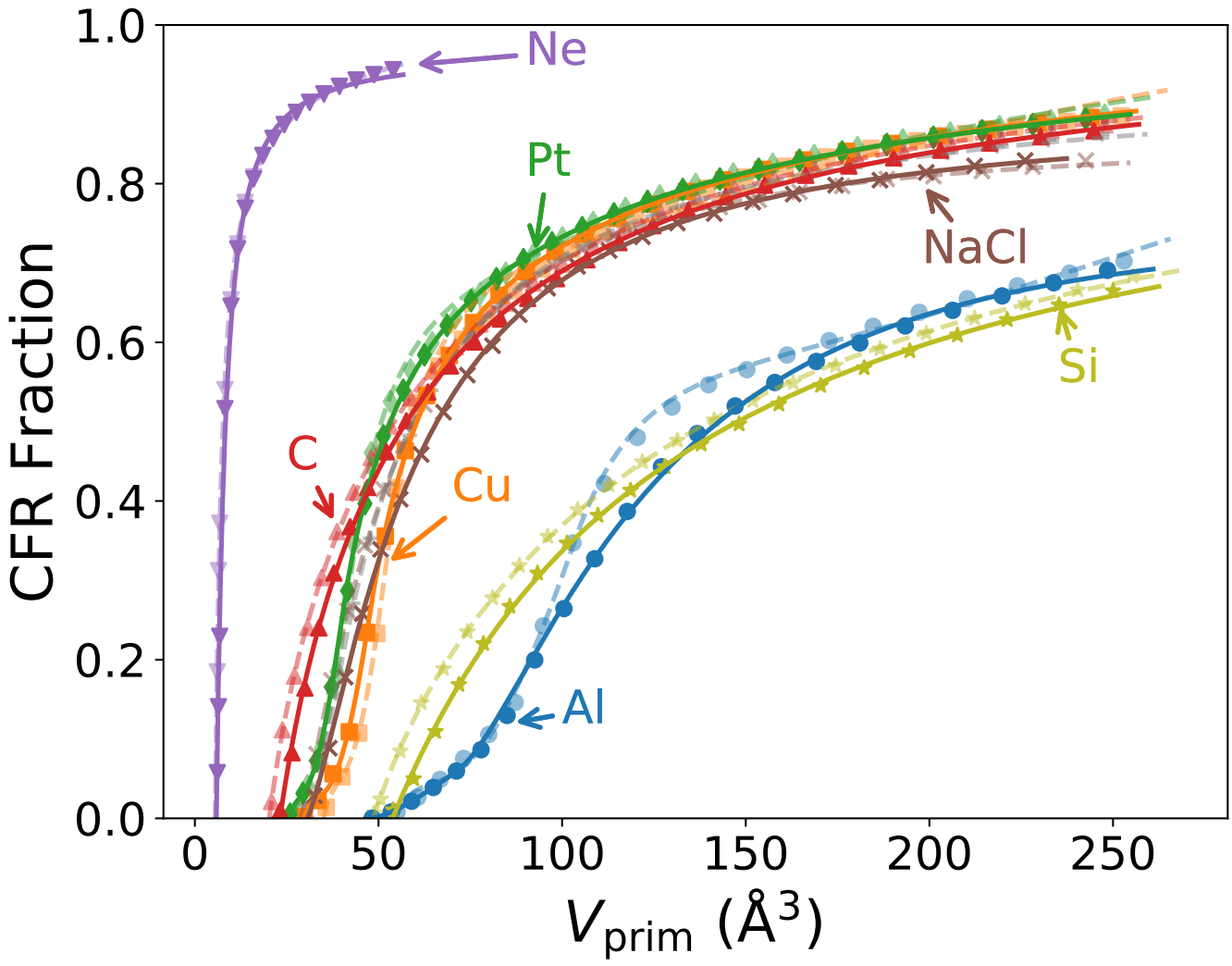

FIG. S4. Emergence of LSDA (solid lines) and PBE (dashed faint lines) CFRs in Al (blue closed circles), Cu (yellow squares), Pt (green diamonds), C (red point-up triangles), Ne (purple point-down triangles), NaCl (brown crosses), and Si (olive stars) as a function of the lattice constant. All lines are fits given in Table II in the main text. For the elemental insulators, the difference between the LSDA and PBE curves has the same sign. For the metals and NaCl, the LSDA and PBE curves cross.

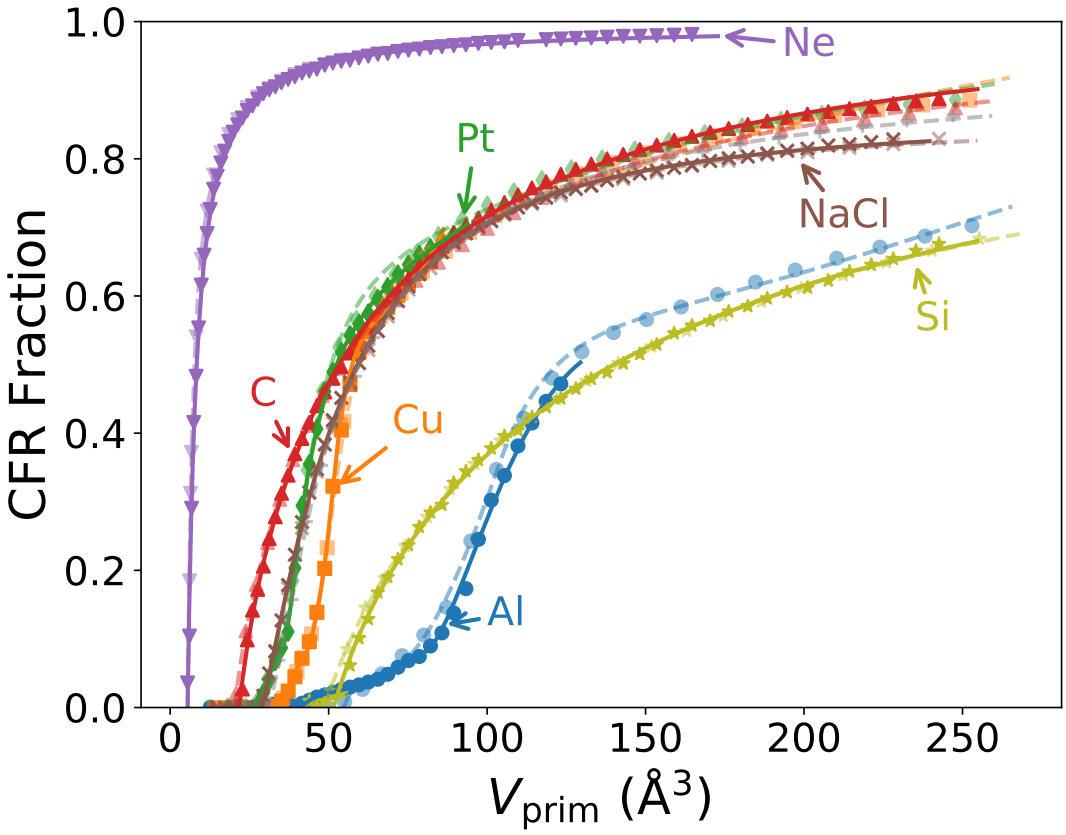

FIG. S5. Comparison between VASP and Castep results for PBE for the elements presented in the main text.

Solid (struc.)	c_0	c_1	c_2	c_3	R^2	V_c (Å^3)
Al (fcc)	0.84	-2.89	3.47	-1.42	0.0010	41.33
	-2.69	27.97	-76.55	63.47		80.52
Cu (fcc)	21.42	-70.61	78.14	-28.95	0.0011	36.43
	6.71	-32.96	59.87	-36.80		51.49
Pt (fcc)	20.24	-67.48	75.43	-28.19	0.0008	28.89
	1.22	-2.94	5.52	-4.64		39.42
C (ds)	1.04	-1.73	1.18	-0.50	0.0015	21.71
Ne (fcc)	0.99	-0.46	-0.29	-0.25	0.0061	5.49
NaCl (rs)	0.86	-0.09	-1.85	1.09	0.0005	28.89
Si (ds)	0.97	-1.63	1.19	-0.52	0.0014	51.54

TABLE S1. Fits for the solids presented in the main text as calculated with PBE in Castep. Materials with two lines of fit parameters use a separate fit for $V_{\text{prim}} < V_0$ (first line) and $V_{\text{prim}} \geq V_0$ (second) line. For these, V_c is given on the first line, and V_0 is given on the second. For the fitting method and fit functions, refer to the main text. The fitted values of V_c for Ne and Si are too large, and the fitted value of V_c for Al is too small; all other values of V_c are within their respective bounds from the numerical calculations.

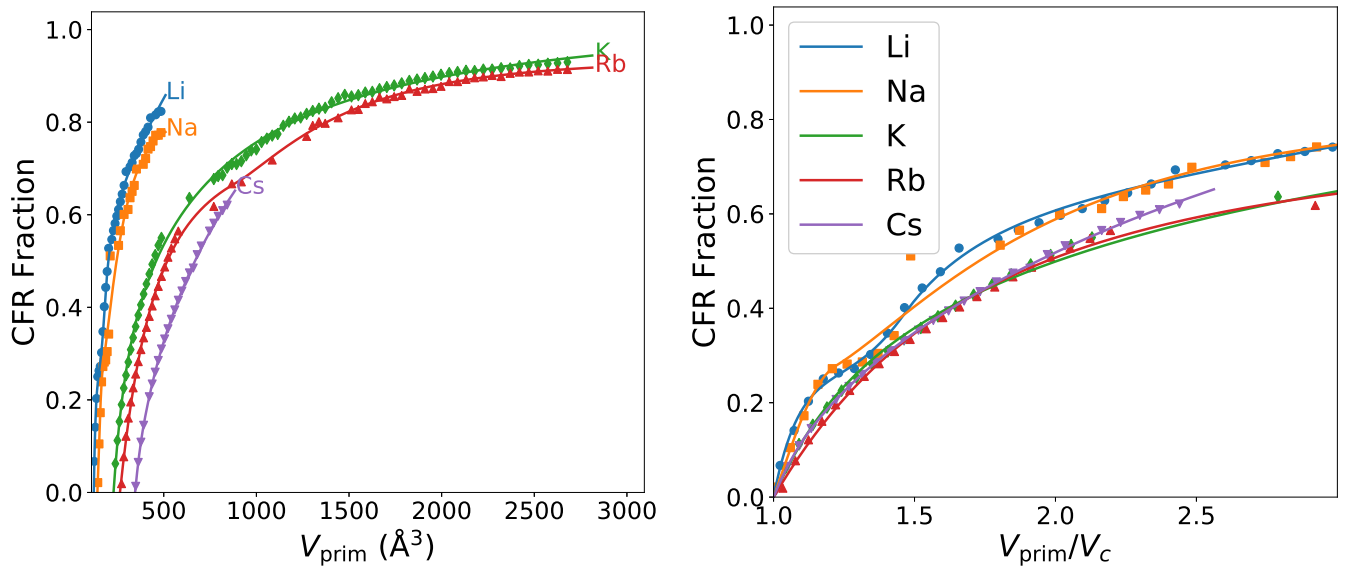

FIG. S6. Fitted CFR strain curves, in dimensioned (left) and dimensionless (right) forms, for Group 1 (alkali metals) elemental solids as calculated with PBE in Castep.

Solid (struc.)	c_0	c_1	c_2	c_3	R^2	V_c (Å^3)	V_c/V_{at}
Li (bcc)	13.64	-48.14	58.39	-23.89	0.0032	122.20	1.50
	1.51	-4.29	7.92	-5.93		178.48	
Na (bcc)	-20.95	70.29	-76.07	26.73	0.0180	141.92	1.37
	0.66	1.52	-4.77	2.85		173.11	
K (bcc)	1.07	-1.67	1.50	-0.90	0.0056	228.89	1.18
Rb (bcc)	0.79	-0.11	-1.14	0.46	0.0023	263.60	1.11
	0.89	1.54	-15.46	26.25		880.56	
Cs (bcc)	-1.43	5.39	-5.04	1.08	0.0002	345.21	
	1.41	-2.72	2.41	-1.08		391.33	

TABLE S2. Fit parameters for the Group 1 (alkali metals) elemental solids as calculated with PBE in Castep. Materials with two lines of fit parameters use a separate fit for $V_{\text{prim}} < V_0$ (first line) and $V_{\text{prim}} \geq V_0$ (second) line. For these, V_c is given on the first line, and V_0 is given on the second. For the fitting method and fit functions, refer to the main text. All values of V_c are within their respective bounds from the numerical calculations. When possible, we report the ratio V_c/V_{at}, with $V_{\text{at}} = 4\pi r_{\text{TS}}^3/3$, a sphere at the non-relativistic turning surface radius r_{TS} as reported in Ref. [10].

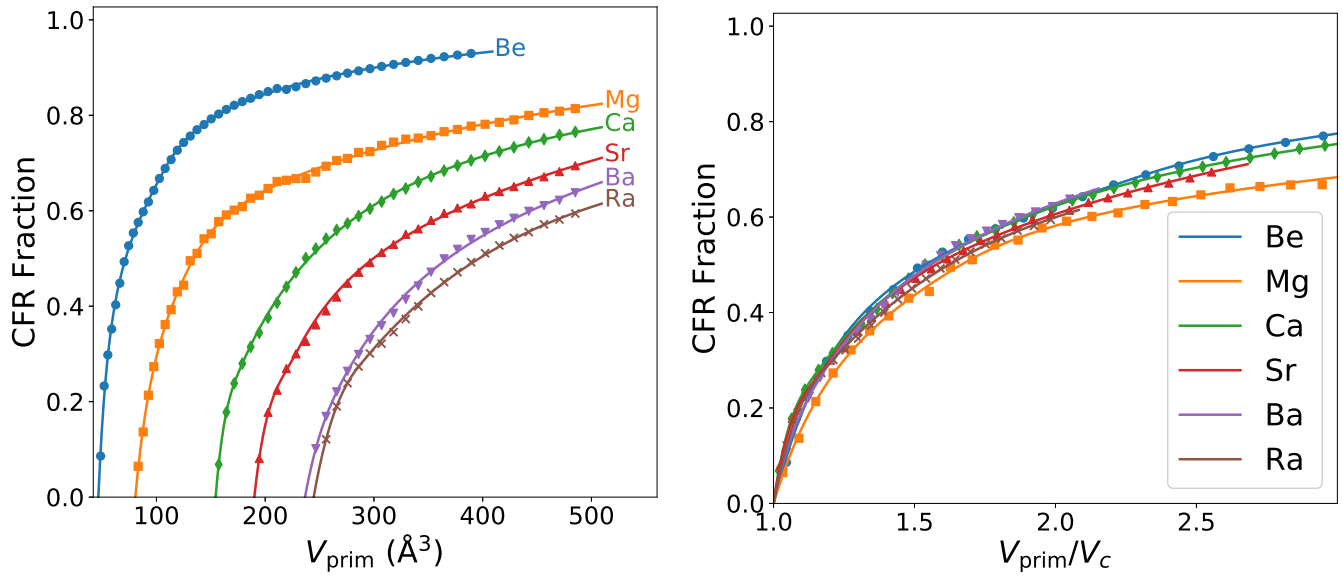

FIG. S7. Fitted CFR strain curves, in dimensioned (left) and dimensionless (right) forms, for Group 2 (alkali earth metals) elemental solids as calculated with PBE in Castep.

Solid (struc.)	c_0	c_1	c_2	c_3	R^2	V_c (Å^3)	V_c/V_{at}
Be (bcc)	1.67	-4.08	5.56	-3.15	0.0011	46.55	1.94
	1.06	-1.39	2.89	-3.84		108.23	
Mg (bcc)	1.86	-4.58	5.56	-2.84	0.0009	80.54	1.86
	1.06	-1.97	3.52	-2.98		133.80	
Ca (fcc)	43.72	-147.30	167.62	-64.05	0.0004	154.37	1.66
	0.97	-0.59	-0.17	-0.09		178.96	
Sr (fcc)	38.23	-129.32	147.96	-56.87	0.0007	189.97	1.55
	1.24	-2.16	2.63	-1.67		229.06	
Ba (bcc)	17.22	-56.94	65.16	-25.43	0.0007	236.59	
	1.20	-1.68	1.62	-1.09		275.68	
Ra (bcc)	8.39	-30.21	38.44	-16.62	0.0003	244.61	
	0.71	0.57	-2.02	0.89		285.89	

TABLE S3. Fit parameters for the Group 2 (alkali earth metals) elemental solids as calculated with PBE in Castep. Materials with two lines of fit parameters use a separate fit for $V_{\text{prim}} < V_0$ (first line) and $V_{\text{prim}} \geq V_0$ (second) line. For these, V_c is given on the first line, and V_0 is given on the second. For the fitting method and fit functions, refer to the main text. The fitted values of V_c for Ba and Ra are too small; all other values of V_c are within their respective bounds from the numerical calculations. When possible, we report the ratio V_c/V_{at}, with $V_{\text{at}} = 4\pi r_{\text{TS}}^3/3$, a sphere at the non-relativistic turning surface radius r_{TS} as reported in Ref. [10].

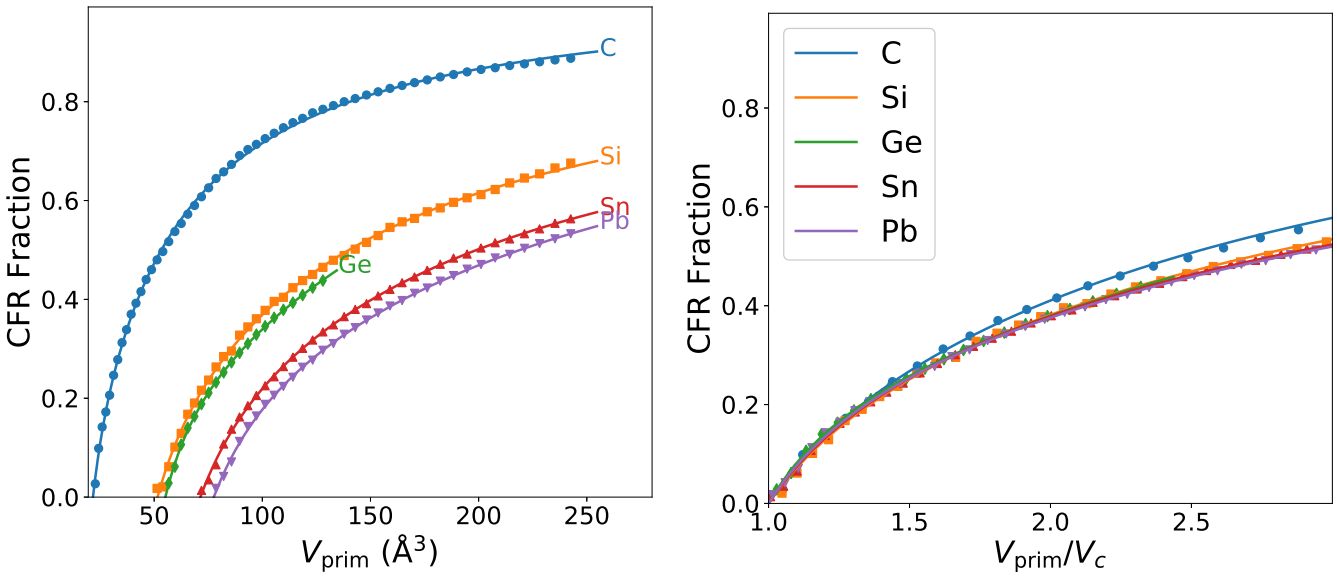

FIG. S8. Fitted CFR strain curves, in dimensioned (left) and dimensionless (right) forms, for Group 14 (carbon group) elemental solids as calculated with PBE in Castep.

Solid (struc.)	c_0	c_1	c_2	c_3	R^2	V_c (Å^3)	V_c/V_{at}
C (ds)	1.04	-1.73	1.18	-0.50	0.0015	21.71	1.57
Si (ds)	0.97	-1.63	1.19	-0.52	0.0014	51.54	1.24
Ge (ds)	1.09	-2.31	2.34	-1.12	0.0001	55.17	1.22
Sn (ds)	0.93	-1.56	1.17	-0.54	0.0003	71.37	1.17
Pb (ds)	0.95	-1.69	1.42	-0.69	0.0003	77.56	

TABLE S4. Fit parameters for the Group 14 (carbon group) elemental solids as calculated with PBE in Castep. The fitted V_c for Si is too large; all other values of V_c are within their respective bounds from the numerical calculations. When possible, we report the ratio V_c/V_{at}, with $V_{\text{at}} = 4\pi r_{\text{TS}}^3/3$, a sphere at the non-relativistic turning surface radius r_{TS} as reported in Ref. [10].

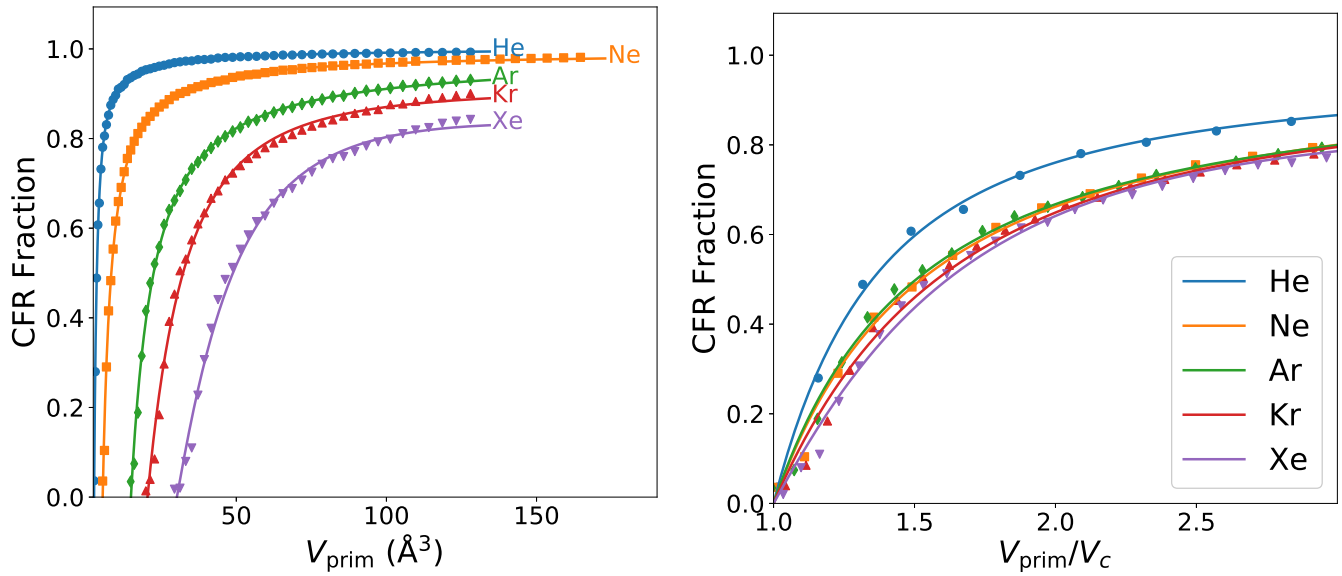

FIG. S9. Fitted CFR strain curves, in dimensioned (left) and dimensionless (right) forms, for Group 18 (rare gases) elemental solids as calculated with PBE in Castep.

Solid (struc.)	c_0	c_1	c_2	c_3	R^2	V_c (Å^3)	V_c/V_{at}
He (fcc)	1.00	-0.40	0.27	-0.87	0.0013	2.63	2.63
Ne (fcc)	0.99	-0.46	-0.29	-0.25	0.0061	5.49	1.99
Ar (fcc)	0.98	-0.45	-0.19	-0.34	0.0072	14.91	1.66
Kr (fcc)	0.91	0.11	-1.48	0.46	0.0139	20.43	1.54
Xe (fcc)	0.74	1.03	-3.15	1.38	0.0128	30.21	1.44

TABLE S5. Fit parameters for the Group 18 (rare gas) elemental solids as calculated with PBE in Castep. All fitted values of V_c are too large, except for He. When possible, we report the ratio V_c/V_{at}, with $V_{\text{at}} = 4\pi r_{\text{TS}}^3/3$, a sphere at the non-relativistic turning surface radius r_{TS} as reported in Ref. [10].

S1. RAW DATA FOR ELEMENTS EMPHASIZED IN MAIN TEXT

TABLE S6: Raw data for Al as calculated with PBE in VASP.

V_{prim} (Å^3)	CFR fraction	Band gap from DOS (eV)
16.4848	0.0000	0.0000
19.0563	0.0000	0.0000
21.8821	0.0000	0.0000
24.9743	0.0000	0.0000
28.3450	0.0000	0.0000
32.0060	0.0000	0.0000
35.9695	0.0000	0.0000
40.2473	0.0000	0.0000
44.8515	0.0000	0.0000
49.7942	0.0000	0.0000
55.0872	0.0081	0.0000
60.7427	0.0264	0.0000
66.7725	0.0491	0.0000
73.1887	0.0756	0.0000
80.0034	0.1056	0.0000
87.2284	0.1461	0.0000
94.8759	0.2427	0.0000
102.9577	0.3472	0.0000
111.4859	0.4219	0.0000
120.4726	0.4801	0.0000
129.9296	0.5185	0.0000
139.8691	0.5466	0.0000
150.3029	0.5656	0.0000
161.2431	0.5840	0.0000
172.7018	0.6022	0.0000
184.6908	0.6202	0.0000
197.2223	0.6378	0.0000
210.3081	0.6550	0.0000
223.9603	0.6712	0.0000
238.1910	0.6872	0.0000
253.0120	0.7024	0.0000

TABLE S7: Raw data for Cu as calculated with PBE in VASP.

V_{prim} (Å^3)	CFR fraction	Band gap from DOS (eV)
11.9580	0.0000	0.0000
14.0455	0.0000	0.0000
16.3627	0.0000	0.0000
18.9217	0.0000	0.0000
21.7346	0.0000	0.0000
24.8132	0.0000	0.0000
28.1696	0.0000	0.0000
31.8159	0.0000	0.0000
35.7639	0.0140	0.0000
40.0258	0.0523	0.0000
44.6134	0.1074	0.0000
49.5388	0.2328	0.0000
54.8141	0.4168	0.0000
60.4511	0.5237	0.0000
66.4619	0.5701	0.0000
72.8586	0.6038	0.0000
79.6530	0.6353	0.0000
86.8572	0.6651	0.0000
94.4833	0.6925	0.0000
102.5431	0.7171	0.0000
111.0487	0.7396	0.0000
120.0122	0.7599	0.0000
129.4454	0.7782	0.0000
139.3604	0.7944	0.0000
149.7693	0.8086	0.0000
160.6839	0.8219	0.0000
172.1163	0.8337	0.0000
184.0786	0.8446	0.0000
196.5826	0.8541	0.0000
209.6405	0.8632	0.0000
223.2641	0.8713	0.0000
237.4655	0.8785	0.0000
252.2568	0.8855	0.0000

TABLE S8: Raw data for Pt as calculated with PBE in VASP.

V_{prim} (Å^3)	CFR fraction	Band gap from DOS (eV)
15.6427	0.0000	0.0000
18.1279	0.0000	0.0000
20.8634	0.0000	0.0000
23.8610	0.0000	0.0000
27.1328	0.0059	0.0000
30.6909	0.0411	0.0000
34.5471	0.0890	0.0000
38.7135	0.1846	0.0000
43.2022	0.3464	0.0000
48.0250	0.4608	0.0000
53.1940	0.5255	0.0000
58.7213	0.5652	0.0000
64.6187	0.5994	0.0000
70.8983	0.6311	0.0000
77.5722	0.6605	0.0000
84.6522	0.6871	0.0000
92.1505	0.7105	0.0000
100.0789	0.7317	0.0000
108.4495	0.7510	0.0000
117.2744	0.7687	0.0000
126.5654	0.7844	0.0000
136.3346	0.7990	0.0000
146.5941	0.8121	0.0000
157.3557	0.8244	0.0000
168.6315	0.8355	0.0000
180.4336	0.8457	0.0000
192.7738	0.8550	0.0000
205.6642	0.8637	0.0000
219.1169	0.8718	0.0000
233.1437	0.8793	0.0000
247.7567	0.8863	0.0000

TABLE S9: Raw data for C as calculated with PBE in VASP.

V_{prim} (Å^3)	CFR fraction	Band gap from DOS (eV)
11.3748	0.0000	4.1395
13.3957	0.0000	3.7061
15.6427	0.0000	3.4592
18.1279	0.0000	3.0474
20.8634	0.0212	2.3060
23.8610	0.1116	0.5534
27.1328	0.1794	0.0000
30.6909	0.2407	0.0000
34.5471	0.3036	0.0000
38.7135	0.3615	0.0000
43.2022	0.4113	0.0000
48.0250	0.4548	0.0000
53.1940	0.4946	0.0000
58.7213	0.5302	0.0000
64.6187	0.5637	0.0000
70.8983	0.5943	0.0000
77.5722	0.6228	0.0000
84.6522	0.6492	0.0000
92.1505	0.6747	0.0000
100.0789	0.6986	0.0000
108.4495	0.7214	0.0000
117.2744	0.7436	0.0000
126.5654	0.7654	0.0000
136.3346	0.7839	0.0000
146.5941	0.7981	0.0000
157.3557	0.8104	0.0000
168.6315	0.8217	0.0000
180.4336	0.8321	0.0000
192.7738	0.8421	0.0000
205.6642	0.8509	0.0000
219.1169	0.8593	0.0000
233.1437	0.8669	0.0000
247.7567	0.8743	0.0000

TABLE S10: Raw data for Ne as calculated with PBE in VASP.

V_{prim} (Å^3)	CFR fraction	Band gap from DOS (eV)
5.7873	0.0933	18.5758
6.0972	0.1847	17.9035
6.4181	0.3122	17.5081
6.7500	0.3719	16.9491
8.1920	0.5404	14.9407
9.8260	0.6535	13.8288
11.6640	0.7240	12.9718
13.7180	0.7763	12.4658
16.0000	0.8088	12.1625
18.5220	0.8356	11.7600
21.2960	0.8570	11.5588
24.3340	0.8745	11.4974
27.6480	0.8899	11.2233
31.2500	0.9024	11.2782
35.1520	0.9131	11.2431
39.3660	0.9227	11.3382
43.9040	0.9306	11.3177
48.7780	0.9373	11.3249
54.0000	0.9436	11.3459

TABLE S11: Raw data for NaCl as calculated with PBE in VASP.

V_{prim} (Å^3)	CFR fraction	Band gap from DOS (eV)
12.6633	0.0000	0.2540
14.8297	0.0000	2.3167
17.2302	0.0000	3.8483
19.8767	0.0000	4.9494
22.7813	0.0000	5.9849
25.9558	0.0000	6.6959
29.4123	0.0134	7.1671
33.1627	0.0809	6.5604
37.2193	0.1739	5.9844
41.5938	0.2617	5.3491
46.2983	0.3438	4.9802
51.3447	0.4150	4.5501
56.7452	0.4699	4.3312
62.5117	0.5212	4.0477
68.6562	0.5700	3.7484
75.1907	0.6093	3.6438
82.1273	0.6404	3.3609
89.4778	0.6765	3.3206
97.2542	0.6987	3.0762
105.4688	0.7181	3.0424
114.1333	0.7342	2.9033
123.2598	0.7463	2.6795
132.8603	0.7611	2.6415
142.9468	0.7705	2.5432
153.5312	0.7796	2.4179
164.6258	0.7896	2.2904
176.2422	0.7971	2.1310
188.3928	0.8059	2.1254
201.0893	0.8094	1.9031
214.3438	0.8160	1.7761
228.1683	0.8215	1.6488
242.5748	0.8291	1.6157

TABLE S12: Raw data for Si as calculated with PBE in VASP.

V_{prim} (Å^3)	CFR fraction	Band gap from DOS (eV)
40.9168	0.0000	0.5507
45.5711	0.0000	0.7547
48.7857	0.0064	0.8074
50.5655	0.0242	0.7107
55.9121	0.0849	0.0000
61.6230	0.1457	0.0000
67.7100	0.1885	0.0000
74.1852	0.2351	0.0000
81.0607	0.2779	0.0000
88.3483	0.3186	0.0000
96.0601	0.3554	0.0000
104.2082	0.3890	0.0000
112.8044	0.4199	0.0000
121.8609	0.4493	0.0000
131.3895	0.4764	0.0000
141.4023	0.5022	0.0000
151.9114	0.5264	0.0000
162.9286	0.5491	0.0000
174.4660	0.5709	0.0000
186.5357	0.5916	0.0000
199.1495	0.6114	0.0000
212.3195	0.6304	0.0000
226.0578	0.6488	0.0000
240.3762	0.6661	0.0000
255.2868	0.6834	0.0000

TABLE S13: Raw data for spin-unpolarized NiO as calculated with PBE in VASP.

V_{prim} (Å^3)	CFR fraction	Band gap from DOS (eV)
17.9978	0.0000	0.0000
20.7205	0.0000	0.0000
23.7047	0.0000	0.0000
26.9625	0.0000	0.0000
30.5060	0.0007	0.0000
34.3470	0.0691	0.0000
38.4977	0.1572	0.0000
42.9699	0.2711	0.0000
47.7757	0.3531	0.0000
52.9272	0.4213	0.0000
58.4362	0.4829	0.0000
64.3149	0.5394	0.0000
70.5751	0.5882	0.0000
77.2289	0.6259	0.0000
84.2884	0.6593	0.0000
91.7654	0.6881	0.0000
99.6721	0.7116	0.0000
108.0203	0.7293	0.0000
116.8221	0.7454	0.0000
126.0896	0.7604	0.2030
135.8346	0.7739	0.0000
146.0693	0.7866	0.0000
156.8055	0.7986	0.2018
168.0553	0.8097	0.1669
179.8308	0.8203	0.0000
192.1438	0.8300	0.0000
205.0065	0.8389	0.1942
218.4307	0.8476	0.1132
232.4285	0.8553	0.1173
247.0120	0.8628	0.0000

TABLE S14: Raw data for Al as calculated with LSDA in VASP.

V_{prim} (Å^3)	CFR fraction	Band gap from DOS (eV)
15.7612	0.0000	0.0000
18.2587	0.0000	0.0000
21.0069	0.0000	0.0000
24.0180	0.0000	0.0000
27.3038	0.0000	0.0000
30.8765	0.0000	0.0000
34.7480	0.0000	0.0000
38.9302	0.0000	0.0000
43.4353	0.0000	0.0000
48.2751	0.0002	0.0000
53.4618	0.0081	0.0000
59.0073	0.0215	0.0000
64.9235	0.0390	0.0000
71.2226	0.0597	0.0000
77.9164	0.0865	0.0000
85.0171	0.1297	0.0000
92.5366	0.1997	0.0000
100.4868	0.2644	0.0000
108.8799	0.3272	0.0000
117.7277	0.3868	0.0000
127.0424	0.4432	0.0000
136.8359	0.4850	0.0000
147.1201	0.5199	0.0000
157.9072	0.5494	0.0000
169.2090	0.5759	0.0000
181.0377	0.5993	0.0000
193.4052	0.6207	0.0000
206.3234	0.6403	0.0000
219.8045	0.6585	0.0000
233.8603	0.6751	0.0000
248.5030	0.6908	0.0000

TABLE S15: Raw data for Cu as calculated with LSDA in VASP.

V_{prim} (Å^3)	CFR fraction	Band gap from DOS (eV)
10.9036	0.0000	0.0000
12.8697	0.0000	0.0000
15.0591	0.0000	0.0000
17.4836	0.0000	0.0000
20.1554	0.0000	0.0000
23.0864	0.0000	0.0000
26.2885	0.0000	0.0000
29.7739	0.0020	0.0000
33.5544	0.0225	0.0000
37.6422	0.0562	0.0000
42.0492	0.1090	0.0000
46.7873	0.2345	0.0000
51.8687	0.3557	0.0000
57.3052	0.4634	0.0000
63.1090	0.5328	0.0000
69.2920	0.5834	0.0000
75.8661	0.6249	0.0000
82.8435	0.6593	0.0000
90.2360	0.6889	0.0000
98.0558	0.7143	0.0000
106.3148	0.7367	0.0000
115.0249	0.7564	0.0000
124.1983	0.7742	0.0000
133.8468	0.7902	0.0000
143.9826	0.8047	0.0000
154.6176	0.8180	0.0000
165.7637	0.8299	0.0000
177.4331	0.8408	0.0000
189.6376	0.8506	0.0000
202.3894	0.8600	0.0000
215.7004	0.8685	0.0000
229.5825	0.8763	0.0000
244.0479	0.8835	0.0000

TABLE S16: Raw data for Pt as calculated with LSDA in VASP.

V_{prim} (Å^3)	CFR fraction	Band gap from DOS (eV)
14.8297	0.0000	0.0000
17.2302	0.0000	0.0000
19.8767	0.0000	0.0000
22.7813	0.0000	0.0000
25.9558	0.0052	0.0000
29.4123	0.0314	0.0000
33.1627	0.0724	0.0000
37.2193	0.1653	0.0000
41.5938	0.2868	0.0000
46.2983	0.3966	0.0000
51.3447	0.4821	0.0000
56.7452	0.5396	0.0000
62.5117	0.5843	0.0000
68.6562	0.6213	0.0000
75.1907	0.6525	0.0000
82.1273	0.6802	0.0000
89.4778	0.7042	0.0000
97.2542	0.7253	0.0000
105.4688	0.7445	0.0000
114.1333	0.7620	0.0000
123.2598	0.7777	0.0000
132.8603	0.7928	0.0000
142.9468	0.8059	0.0000
153.5312	0.8182	0.0000
164.6258	0.8295	0.0000
176.2422	0.8400	0.0000
188.3928	0.8494	0.0000
201.0893	0.8584	0.0000
214.3438	0.8667	0.0000
228.1683	0.8746	0.0000
242.5748	0.8817	0.0000

TABLE S17: Raw data for C as calculated with LSDA in VASP.

V_{prim} (Å^3)	CFR fraction	Band gap from DOS (eV)
10.9967	0.0000	4.0588
12.9738	0.0000	3.7563
15.1746	0.0000	3.3818
17.6112	0.0000	3.0743
20.2957	0.0000	2.5228
23.2399	0.0097	1.0881
26.4560	0.0827	0.0000
29.9558	0.1643	0.0000
33.7514	0.2401	0.0000
37.8549	0.3093	0.0000
42.2781	0.3676	0.0000
47.0331	0.4171	0.0000
52.1320	0.4621	0.0000
57.5866	0.5012	0.0000
63.4090	0.5374	0.0000
69.6113	0.5703	0.0000
76.2053	0.6005	0.0000
83.2031	0.6294	0.0000
90.6168	0.6555	0.0000
98.4582	0.6803	0.0000
106.7394	0.7041	0.0000
115.4725	0.7258	0.0000
124.6693	0.7471	0.0000
134.3419	0.7665	0.0000
144.5024	0.7837	0.0000
155.1626	0.7981	0.0000
166.3347	0.8106	0.0000
178.0305	0.8224	0.0000
190.2621	0.8327	0.0000
203.0416	0.8422	0.0000
216.3808	0.8512	0.0000
230.2918	0.8591	0.0000
244.7867	0.8666	0.0000

TABLE S18: Raw data for Ne as calculated with LSDA in VASP.

V_{prim} (Å^3)	CFR fraction	Band gap from DOS (eV)
5.7873	0.0261	18.3436
6.0972	0.0576	17.6710
6.4181	0.1407	17.0007
6.7500	0.2294	16.4522
8.1920	0.5164	14.4664
9.8260	0.6455	13.4261
11.6640	0.7178	12.4733
13.7180	0.7691	11.9869
16.0000	0.8060	11.6004
18.5220	0.8354	11.3754
21.2960	0.8570	11.3931
24.3340	0.8745	11.3476
27.6480	0.8899	11.2333
31.2500	0.9024	11.3534
35.1520	0.9131	11.3287
39.3660	0.9227	11.4308
43.9040	0.9306	11.5933
48.7780	0.9373	11.6459
54.0000	0.9436	11.7969

TABLE S19: Raw data for NaCl as calculated with LSDA in VASP.

V_{prim} (Å^3)	CFR fraction	Band gap from DOS (eV)
10.4455	0.0000	0.0000
12.3577	0.0000	0.0000
14.4902	0.0000	1.7634
16.8548	0.0000	3.2939
19.4636	0.0000	4.4587
22.3287	0.0000	5.4665
25.4619	0.0000	6.1151
28.8753	0.0000	6.7088
32.5810	0.0286	6.2297
36.5908	0.0884	5.5120
40.9168	0.1780	5.0743
45.5711	0.2580	4.5858
50.5655	0.3391	4.2189
55.9121	0.4023	3.9347
61.6230	0.4586	3.7337
67.7100	0.5119	3.5726
74.1852	0.5587	3.4197
81.0607	0.5957	3.1547
88.3483	0.6348	3.0390
96.0601	0.6682	2.9438
104.2082	0.6958	2.8269
112.8044	0.7157	2.7118
121.8609	0.7331	2.5950
131.3895	0.7504	2.4746
141.4023	0.7623	2.3570
151.9114	0.7769	2.3220
162.9286	0.7869	2.2251
174.4660	0.7982	2.1907
186.5357	0.8045	2.0956
199.1495	0.8142	1.9712
212.3195	0.8224	1.9687
226.0578	0.8293	1.8462

TABLE S20: Raw data for Si as calculated with LSDA in VASP.

V_{prim} (Å^3)	CFR fraction	Band gap from DOS (eV)
39.3660	0.0000	0.3872
43.9040	0.0000	0.6069
48.7780	0.0000	0.6498
54.0000	0.0105	0.1719
59.5820	0.0497	0.0000
65.5360	0.1094	0.0000
71.8740	0.1685	0.0000
78.6080	0.2202	0.0000
85.7500	0.2672	0.0000
93.3120	0.3090	0.0000
101.3060	0.3468	0.0000
109.7440	0.3819	0.0000
118.6380	0.4135	0.0000
128.0000	0.4430	0.0000
137.8420	0.4716	0.0000
148.1760	0.4970	0.0000
159.0140	0.5221	0.0000
170.3680	0.5455	0.0000
182.2500	0.5678	0.0000
194.6720	0.5892	0.0000
207.6460	0.6091	0.0000
221.1840	0.6285	0.0000
235.2980	0.6472	0.0000
250.0000	0.6648	0.0000

TABLE S21: Raw data for Al as calculated with PBE in Castep.

V_{prim} (Å^3)	CFR fraction
3.9062	0.0000
4.3940	0.0000
4.9207	0.0000
5.4880	0.0000
6.0972	0.0000
6.7500	0.0000
7.4478	0.0000
8.1920	0.0000
8.9842	0.0000
9.8260	0.0000
10.7188	0.0000
11.6640	0.0000
12.6633	0.0005
13.7180	0.0000
14.8297	0.0000
16.0000	0.0000
17.2302	0.0000
18.5220	0.0003
19.8767	0.0003
21.2960	0.0003
22.7812	0.0003
24.3340	0.0000
25.9558	0.0003
27.6480	0.0015
29.4123	0.0015
31.2500	0.0015
33.1627	0.0053
35.1520	0.0053
37.2192	0.0053
39.3660	0.0018
41.5938	0.0062
43.9040	0.0107
46.2983	0.0153
48.7780	0.0184
51.3448	0.0222
54.0000	0.0262
56.7452	0.0297
59.5820	0.0330
62.5117	0.0371
65.5360	0.0412
68.6562	0.0484
71.8740	0.0587
75.1908	0.0685
78.6080	0.0744
82.1273	0.0897
85.7500	0.1089
89.4777	0.1378
93.3120	0.1732
97.2542	0.2452
101.3060	0.3023
105.4690	0.3382
109.7440	0.3814
114.1330	0.4149
118.6380	0.4464
123.2600	0.4718

TABLE S22: Raw data for Cu as calculated with PBE in Castep.

V_{prim} (Å^3)	CFR fraction
3.9062	0.0000
4.3940	0.0000
4.9207	0.0000
5.4880	0.0000
6.0972	0.0000
6.7500	0.0000
7.4478	0.0000
8.1920	0.0000
8.9842	0.0000
9.8260	0.0000
10.7188	0.0000
11.6640	0.0000
12.6633	0.0000
13.7180	0.0000
14.8297	0.0000
16.0000	0.0000
17.2302	0.0000
18.5220	0.0000
19.8767	0.0000
21.2960	0.0000
22.7812	0.0000
24.3340	0.0000
25.9558	0.0000
27.6480	0.0000
29.4123	0.0000
31.2500	0.0000
33.1627	0.0019
35.1520	0.0095
37.2192	0.0239
39.3660	0.0448
41.5938	0.0718
43.9040	0.0959
46.2983	0.1387
48.7780	0.2028
51.3448	0.3226
54.0000	0.4044
56.7452	0.4711
59.5820	0.5177
62.5117	0.5479
65.5360	0.5663
68.6562	0.5832
71.8740	0.6008
75.1908	0.6181
78.6080	0.6329
82.1273	0.6500

TABLE S23: Raw data for Pt as calculated with PBE in Castep.

V_{prim} (Å^3)	CFR fraction
4.3940	0.0000
4.9207	0.0000
5.4880	0.0000
6.0972	0.0000
6.7500	0.0000
7.4478	0.0000
8.1920	0.0000
8.9842	0.0000
9.8260	0.0000
10.7188	0.0000
11.6640	0.0000
12.6633	0.0000
13.7180	0.0000
14.8297	0.0000
16.0000	0.0000
17.2302	0.0000
18.5220	0.0000
19.8767	0.0000
21.2960	0.0000
22.7812	0.0000
24.3340	0.0000
25.9558	0.0000
27.6480	0.0040
29.4123	0.0209
31.2500	0.0402
33.1627	0.0680
35.1520	0.0870
37.2192	0.1105
39.3660	0.2034
41.5938	0.2942
43.9040	0.3549
46.2983	0.4063
48.7780	0.4611
51.3448	0.4893
54.0000	0.5179
56.7452	0.5427
59.5820	0.5593
62.5117	0.5743
65.5360	0.5953
68.6562	0.6127
71.8740	0.6310
75.1908	0.6457
78.6080	0.6598
82.1273	0.6692
85.7500	0.6799
89.4777	0.6891

TABLE S24: Raw data for C as calculated with PBE in Castep.

V_{prim} (Å^3)	CFR fraction
3.9062	0.0000
4.3940	0.0000
4.9208	0.0000
5.4880	0.0000
6.0972	0.0000
6.7500	0.0000
7.4478	0.0000
8.1920	0.0000
8.9842	0.0000
9.8260	0.0000
10.7188	0.0000
11.6640	0.0000
12.6633	0.0000
13.7180	0.0000
14.8297	0.0000
16.0000	0.0000
17.2302	0.0000
18.5220	0.0000
19.8767	0.0000
21.2960	0.0015
22.7812	0.0270
24.3340	0.0986
25.9558	0.1420
27.6480	0.1723
29.4122	0.2062
31.2500	0.2465
33.1628	0.2781
35.1520	0.3125
37.2192	0.3388
39.3660	0.3700
41.5938	0.3923
43.9040	0.4157
46.2982	0.4402
48.7780	0.4602
51.3448	0.4800
54.0000	0.4969
56.7452	0.5169
59.5820	0.5373
62.5118	0.5536
65.5360	0.5724
68.6562	0.5900
71.8740	0.6077
75.1908	0.6258
78.6080	0.6447
82.1272	0.6581
85.7500	0.6731
89.4778	0.6911
93.3120	0.7033
97.2542	0.7137
101.3060	0.7253
105.4688	0.7362
109.7440	0.7474
114.1332	0.7576
118.6380	0.7664
123.2598	0.7776
128.0000	0.7847
132.8602	0.7922
137.8420	0.8000
142.9468	0.8063
⋮	⋮

V_{prim} (Å^3)	CFR fraction
⋮	⋮
148.1760	0.8136
153.5312	0.8200
159.0140	0.8269
164.6258	0.8328
170.3680	0.8385
176.2422	0.8441
182.2500	0.8501
188.3928	0.8550
194.6720	0.8603
201.0900	0.8652
207.6460	0.8687
214.3440	0.8731
221.1840	0.8765
228.1680	0.8807
235.2980	0.8844
242.5740	0.8878

TABLE S25: Raw data for Ne as calculated with PBE in Castep.

V_{prim} (Å^3)	CFR fraction
3.9062	0.0000
4.3940	0.0000
4.9207	0.0000
5.4880	0.0359
6.0972	0.1041
6.7500	0.2904
7.4478	0.4156
8.1920	0.4829
8.9842	0.5534
9.8260	0.6158
10.7188	0.6594
11.6640	0.6909
12.6633	0.7259
13.7180	0.7556
14.8297	0.7745
16.0000	0.7939
17.2302	0.8111
18.5220	0.8253
19.8767	0.8388
21.2960	0.8494
22.7812	0.8594
24.3340	0.8702
25.9558	0.8772
27.6480	0.8868
29.4123	0.8949
31.2500	0.9007
33.1627	0.9049
35.1520	0.9111
37.2192	0.9157
39.3660	0.9197
41.5938	0.9249
43.9040	0.9280
46.2983	0.9307
48.7780	0.9364
51.3448	0.9396
54.0000	0.9422
56.7452	0.9436
59.5820	0.9470
62.5117	0.9497
65.5360	0.9525
68.6562	0.9535
71.8740	0.9565
75.1908	0.9583
78.6080	0.9599
82.1273	0.9621
85.7500	0.9634
89.4777	0.9650
93.3120	0.9661
97.2542	0.9682
101.3060	0.9694
105.4690	0.9704
109.7440	0.9725
118.6380	0.9737
123.2600	0.9746
128.0000	0.9755
132.8600	0.9762
137.8420	0.9773
142.9470	0.9785
148.1760	0.9787
⋮	⋮

V_{prim} (Å^3)	CFR fraction
⋮	⋮
153.5310	0.9795
159.0140	0.9802
164.6260	0.9812

TABLE S26: Raw data for NaCl as calculated with PBE in Castep.

V_{prim} (Å^3)	CFR fraction
4.3940	0.0000
4.9208	0.0000
5.4880	0.0000
6.0972	0.0000
6.7500	0.0000
7.4478	0.0000
8.1920	0.0000
8.9842	0.0000
9.8260	0.0000
10.7188	0.0000
11.6640	0.0000
12.6633	0.0000
13.7180	0.0000
14.8297	0.0000
16.0000	0.0000
17.2302	0.0000
18.5220	0.0000
19.8767	0.0000
21.2960	0.0000
22.7812	0.0000
24.3340	0.0000
25.9558	0.0000
27.6480	0.0009
29.4122	0.0171
31.2500	0.0497
33.1628	0.0822
35.1520	0.1270
37.2192	0.1784
39.3660	0.2227
41.5938	0.2703
43.9040	0.3135
46.2982	0.3475
48.7780	0.3835
51.3448	0.4188
54.0000	0.4515
56.7452	0.4743
59.5820	0.5021
62.5118	0.5274
65.5360	0.5488
68.6562	0.5751
71.8740	0.5927
75.1908	0.6137
78.6080	0.6318
82.1272	0.6503
85.7500	0.6638
89.4778	0.6783
93.3120	0.6913
97.2542	0.7011
101.3060	0.7092
105.4688	0.7202
109.7440	0.7289
114.1332	0.7364
118.6380	0.7433
123.2598	0.7509
128.0000	0.7559
132.8602	0.7608
137.8420	0.7687
142.9468	0.7736
148.1760	0.7785
⋮	⋮

V_{prim} (Å^3)	CFR fraction
⋮	⋮
153.5312	0.7830
159.0140	0.7870
164.6258	0.7908
170.3680	0.7968
176.2422	0.8008
182.2500	0.8032
188.3928	0.8078
194.6720	0.8117
201.0900	0.8148
207.6460	0.8194
214.3440	0.8211
221.1840	0.8243
228.1680	0.8283

TABLE S27: Raw data for Si as calculated with PBE in Castep.

V_{prim} (Å^3)	CFR fraction
3.9062	0.0000
4.3940	0.0000
4.9208	0.0000
5.4880	0.0000
6.0972	0.0000
6.7500	0.0000
7.4478	0.0000
8.1920	0.0000
8.9842	0.0000
9.8260	0.0000
10.7188	0.0000
11.6640	0.0000
12.6633	0.0000
13.7180	0.0000
14.8297	0.0000
16.0000	0.0000
17.2302	0.0000
18.5220	0.0000
19.8767	0.0000
21.2960	0.0000
22.7812	0.0000
24.3340	0.0000
25.9558	0.0000
27.6480	0.0000
29.4122	0.0000
31.2500	0.0000
33.1628	0.0000
35.1520	0.0000
37.2192	0.0000
39.3660	0.0000
41.5938	0.0000
43.9040	0.0095
46.2982	0.0020
48.7780	0.0093
51.3448	0.0176
54.0000	0.0208
56.7452	0.0614
59.5820	0.1012
62.5118	0.1289
65.5360	0.1677
68.6562	0.1903
71.8740	0.2162
75.1908	0.2368
78.6080	0.2632
82.1272	0.2843
85.7500	0.2955
89.4778	0.3277
93.3120	0.3444
97.2542	0.3609
101.3060	0.3779
105.4688	0.3959
109.7440	0.4042
114.1332	0.4236
118.6380	0.4381
123.2598	0.4504
128.0000	0.4648
132.8602	0.4792
137.8420	0.4887
142.9468	0.5017
⋮	⋮
148.1760	0.5154
153.5312	0.5292
159.0140	0.5456
164.6258	0.5569
170.3680	0.5639
176.2422	0.5773
182.2500	0.5851
188.3928	0.5964
194.6720	0.6056
201.0900	0.6121
207.6460	0.6224
214.3440	0.6357
221.1840	0.6455
228.1680	0.6540
235.2980	0.6659
242.5740	0.6758

S2. RAW DATA FOR GROUP 1 ELEMENTAL SOLIDS

TABLE S28: Raw data for Li as calculated with PBE in Castep.

V_{prim} (Å^3)	CFR fraction
4.0000	0.0000
4.6305	0.0000
5.3240	0.0000
6.0835	0.0000
6.9120	0.0000
7.8125	0.0000
8.7880	0.0000
9.8415	0.0000
10.9760	0.0000
12.1945	0.0000
13.5000	0.0000
14.8955	0.0000
16.3840	0.0000
17.9685	0.0000
19.6520	0.0000
21.4375	0.0000
23.3280	0.0000
25.3265	0.0000
27.4360	0.0000
29.6595	0.0000
32.0000	0.0000
34.4605	0.0000
37.0440	0.0000
39.7535	0.0000
42.5920	0.0000
45.5625	0.0000
48.6680	0.0000
51.9115	0.0000
55.2960	0.0000
58.8245	0.0000
62.5000	0.0000
66.3255	0.0000
70.3040	0.0000
74.4385	0.0000
78.7320	0.0000
83.1875	0.0000
87.8080	0.0000
92.5965	0.0000
97.5560	0.0000
102.6900	0.0000
108.0000	0.0000
113.4900	0.0000
119.1640	0.0028
125.0230	0.0671
131.0720	0.1410
137.3120	0.2031
143.7480	0.2503
150.3820	0.2630
157.2160	0.2723
164.2550	0.3022
171.5000	0.3476
178.9550	0.4014
186.6240	0.4430
194.5080	0.4774
202.6120	0.5276
219.4880	0.5466
⋮	⋮

V_{prim} (Å^3)	CFR fraction
⋮	⋮
228.2670	0.5659
237.2760	0.5813
246.5200	0.5970
256.0000	0.6112
265.7200	0.6282
275.6840	0.6445
285.8940	0.6634
296.3520	0.6932
318.0280	0.7038
329.2510	0.7128
340.7360	0.7276
352.4850	0.7322
364.5000	0.7415
376.7850	0.7568
389.3440	0.7724
402.1790	0.7798
415.2920	0.7893
428.6880	0.8095
456.3360	0.8159
470.5960	0.8223
485.1500	0.8233

TABLE S29: Raw data for Na as calculated with PBE in Castep.

V_{prim} (Å^3)	CFR fraction
4.0000	0.0000
4.6305	0.0000
5.3240	0.0000
6.0835	0.0000
6.9120	0.0000
7.8125	0.0000
8.7880	0.0000
9.8415	0.0000
10.9760	0.0000
12.1945	0.0000
13.5000	0.0000
14.8955	0.0000
16.3840	0.0000
17.9685	0.0000
19.6520	0.0000
21.4375	0.0000
23.3280	0.0000
25.3265	0.0000
27.4360	0.0000
29.6595	0.0000
32.0000	0.0000
34.4605	0.0000
37.0440	0.0000
39.7535	0.0000
42.5920	0.0000
45.5625	0.0000
48.6680	0.0000
51.9115	0.0000
55.2960	0.0000
58.8245	0.0000
62.5000	0.0000
66.3255	0.0000
70.3040	0.0000
74.4385	0.0000
78.7320	0.0000
83.1875	0.0000
87.8080	0.0000
92.5965	0.0000
97.5560	0.0000
102.6900	0.0000
108.0000	0.0000
113.4900	0.0000
119.1640	0.0000
125.0230	0.0000
131.0720	0.0000
137.3120	0.0000
143.7480	0.0213
150.3820	0.1049
157.2160	0.1723
164.2550	0.2389
171.5000	0.2721
178.9550	0.2818
186.6240	0.2863
194.5080	0.3044
202.6120	0.3421
210.9380	0.5110
256.0000	0.5337
265.7200	0.5655
285.8940	0.6007
⋮	⋮

V_{prim} (Å^3)	CFR fraction
⋮	⋮
307.0620	0.6113
318.0280	0.6367
329.2510	0.6505
340.7360	0.6633
352.4850	0.6988
389.3440	0.7090
402.1790	0.7214
415.2920	0.7418
428.6880	0.7472
442.3680	0.7594
456.3360	0.7716
470.5960	0.7718
485.1500	0.7774

TABLE S30: Raw data for K as calculated with PBE in Castep.

V_{prim} (Å^3)	CFR fraction
105.2869	0.0000
111.6025	0.0000
118.1657	0.0000
124.9814	0.0000
132.0541	0.0000
139.3888	0.0000
146.9902	0.0000
154.8631	0.0000
163.0121	0.0000
171.4422	0.0000
180.1579	0.0000
189.1642	0.0000
198.4658	0.0000
208.0673	0.0000
217.9736	0.0000
228.1895	0.0090
238.7197	0.0622
249.5690	0.1122
260.7421	0.1531
272.2438	0.1898
284.0789	0.2255
296.2521	0.2532
308.7682	0.2817
321.6319	0.3086
334.8480	0.3344
348.4213	0.3583
362.3565	0.3829
376.6585	0.4054
391.3318	0.4285
406.3815	0.4504
421.8120	0.4719
437.6284	0.4929
453.8352	0.5129
470.4373	0.5340
487.4395	0.5500
638.4292	0.6363
770.1397	0.6772
793.7138	0.6835
817.7633	0.6855
842.2970	0.7017
867.3149	0.7095
892.8169	0.7095
918.8189	0.7157
945.3290	0.7285
972.3311	0.7390
999.8492	0.7412
1027.8832	0.7569
1056.4331	0.7644
1085.5068	0.7710
1115.1123	0.7745
1145.2496	0.7922
1175.9187	0.8009
1207.1434	0.8080
1238.9078	0.8101
1271.2199	0.8179
1304.0956	0.8242
1337.5347	0.8292
1371.5374	0.8311
1406.1116	0.8431
⋮	⋮

V_{prim} (Å^3)	CFR fraction
⋮	⋮
1441.2652	0.8518
1476.9982	0.8590
1513.3106	0.8556
1550.2183	0.8584
1587.7292	0.8640
1625.8274	0.8656
1664.5369	0.8714
1703.8574	0.8759
1743.7892	0.8794
1784.3400	0.8840
1825.5179	0.8892
1867.3228	0.8922
1909.7547	0.8953
1952.8375	0.8986
1996.5553	0.9025
2040.9159	0.9060
2085.9354	0.9085
2131.6136	0.9111
2177.9506	0.9105
2224.9544	0.9137
2272.6327	0.9137
2320.9858	0.9167
2370.0135	0.9162
2419.7317	0.9212
2470.1484	0.9237
2521.2477	0.9241
2573.0534	0.9263
2625.5655	0.9276
2678.7840	0.9298

TABLE S31: Raw data for Rb as calculated with PBE in Castep.

V_{prim} (Å^3)	CFR fraction
105.2869	0.0000
111.6025	0.0000
118.1657	0.0000
124.9814	0.0000
132.0541	0.0000
139.3888	0.0000
146.9902	0.0000
154.8631	0.0000
163.0121	0.0000
171.4422	0.0000
180.1579	0.0000
189.1642	0.0000
198.4658	0.0000
208.0673	0.0000
217.9736	0.0000
228.1895	0.0000
238.7197	0.0000
249.5690	0.0000
260.7421	0.0000
272.2438	0.0190
284.0789	0.0771
296.2521	0.1214
308.7682	0.1607
321.6319	0.1955
334.8480	0.2260
348.4213	0.2558
362.3565	0.2826
376.6585	0.3085
391.3318	0.3340
406.3815	0.3567
421.8120	0.3803
437.6284	0.4028
453.8352	0.4248
470.4373	0.4451
487.4395	0.4667
504.8464	0.4871
522.6629	0.5082
540.8937	0.5279
559.5436	0.5479
578.6173	0.5648
770.1397	0.6180
867.3149	0.6668
918.8189	0.6710
1085.5068	0.7181
1271.2199	0.7692
1304.0956	0.7931
1337.5347	0.8011
1371.5374	0.7976
1441.2652	0.8094
1513.3106	0.8266
1550.2183	0.8274
1587.7292	0.8403
1625.8274	0.8441
1664.5369	0.8540
1703.8574	0.8503
1743.7892	0.8553
1784.3400	0.8577
1825.5179	0.8718
1867.3228	0.8665
⋮	⋮

V_{prim} (Å^3)	CFR fraction
⋮	⋮
1909.7547	0.8716
1952.8375	0.8726
1996.5553	0.8774
2040.9159	0.8877
2085.9354	0.8876
2131.6136	0.8924
2177.9506	0.8958
2224.9544	0.8977
2272.6327	0.9008
2320.9858	0.8986
2370.0135	0.9055
2419.7317	0.9082
2470.1484	0.9084
2521.2477	0.9108
2573.0534	0.9103
2625.5655	0.9140
2678.7840	0.9137

TABLE S32: Raw data for Cs as calculated with PBE in Castep.

V_{prim} (Å^3)	CFR fraction
105.2869	0.0000
111.6025	0.0000
118.1657	0.0000
124.9814	0.0000
132.0541	0.0000
139.3888	0.0000
146.9902	0.0000
154.8631	0.0000
163.0121	0.0000
171.4422	0.0000
180.1579	0.0000
189.1642	0.0000
198.4658	0.0000
208.0673	0.0000
217.9736	0.0000
228.1895	0.0000
238.7197	0.0000
249.5690	0.0000
260.7421	0.0000
272.2438	0.0000
284.0789	0.0000
296.2521	0.0000
308.7682	0.0000
321.6319	0.0000
334.8480	0.0008
348.4213	0.0133
362.3565	0.0649
376.6585	0.1087
391.3318	0.1452
421.8120	0.2068
437.6284	0.2343
453.8352	0.2599
470.4373	0.2852
487.4395	0.3100
504.8464	0.3316
522.6629	0.3536
540.8937	0.3743
559.5436	0.3944
578.6173	0.4154
598.1197	0.4353
618.0554	0.4558
638.4292	0.4744
659.2460	0.4849
680.5104	0.5138
702.2272	0.5325
747.0371	0.5648
770.1397	0.5818
793.7138	0.5968
817.7633	0.6089
842.2970	0.6208

S3. RAW DATA FOR GROUP 2 ELEMENTAL SOLIDS

TABLE S33: Raw data for Be as calculated with PBE in Castep.

V_{prim} (Å^3)	CFR fraction
4.0000	0.0000
4.6305	0.0000
5.3240	0.0000
6.0835	0.0000
6.9120	0.0000
7.8125	0.0000
8.7880	0.0000
9.8415	0.0000
10.9760	0.0000
12.1945	0.0000
13.5000	0.0000
14.8955	0.0000
16.3840	0.0000
17.9685	0.0000
19.6520	0.0000
21.4375	0.0000
23.3280	0.0000
25.3265	0.0000
27.4360	0.0000
29.6595	0.0000
32.0000	0.0000
34.4605	0.0000
37.0440	0.0000
39.7535	0.0000
42.5920	0.0000
45.5625	0.0000
48.6680	0.0860
51.9115	0.2329
55.2960	0.2980
58.8245	0.3521
62.5000	0.4029
66.3255	0.4482
70.3040	0.4933
74.4385	0.5267
78.7320	0.5535
83.1875	0.5755
87.8080	0.5978
92.5965	0.6185
97.5560	0.6427
102.6900	0.6675
108.0000	0.6886
113.4900	0.7072
119.1640	0.7267
125.0230	0.7430
131.0720	0.7564
137.3120	0.7698
143.7480	0.7806
150.3820	0.7926
157.2160	0.8026
164.2550	0.8122
171.5000	0.8210
178.9550	0.8288
186.6240	0.8356
194.5080	0.8433
202.6120	0.8497
210.9380	0.8560
219.4880	0.8542
⋮	⋮
228.2670	0.8597
237.2760	0.8663
246.5200	0.8721
256.0000	0.8779
265.7200	0.8827
275.6840	0.8883
285.8940	0.8930
296.3520	0.8977
307.0620	0.9024
318.0280	0.9066
329.2510	0.9108
340.7360	0.9149
352.4850	0.9192
364.5000	0.9227
376.7850	0.9263
389.3440	0.9295

TABLE S34: Raw data for Mg as calculated with PBE in Castep.

V_{prim} (Å^3)	CFR fraction
4.0000	0.0000
4.6305	0.0000
5.3240	0.0000
6.0835	0.0000
6.9120	0.0000
7.8125	0.0000
8.7880	0.0000
9.8415	0.0000
10.9760	0.0000
12.1945	0.0000
13.5000	0.0000
14.8955	0.0000
16.3840	0.0000
17.9685	0.0000
19.6520	0.0000
21.4375	0.0000
23.3280	0.0000
25.3265	0.0000
27.4360	0.0000
29.6595	0.0000
32.0000	0.0000
34.4605	0.0000
37.0440	0.0000
39.7535	0.0000
42.5920	0.0000
45.5625	0.0000
48.6680	0.0000
51.9115	0.0000
55.2960	0.0000
58.8245	0.0000
62.5000	0.0000
66.3255	0.0000
70.3040	0.0000
74.4385	0.0000
78.7320	0.0333
83.1875	0.0645
87.8080	0.1366
92.5965	0.2134
97.5560	0.2733
102.6900	0.3216
108.0000	0.3615
113.4900	0.3928
119.1640	0.4301
125.0230	0.4440
131.0720	0.4952
137.3120	0.5106
143.7480	0.5413
150.3820	0.5516
157.2160	0.5772
164.2550	0.5913
171.5000	0.6013
178.9550	0.6086
186.6240	0.6263
194.5080	0.6325
202.6120	0.6466
210.9380	0.6612
219.4880	0.6639
228.2670	0.6674
237.2760	0.6679
⋮	⋮
246.5200	0.6812
256.0000	0.6933
265.7200	0.7053
275.6840	0.7097
285.8940	0.7221
296.3520	0.7239
307.0620	0.7369
318.0280	0.7439
329.2510	0.7500
340.7360	0.7523
352.4850	0.7574
364.5000	0.7656
376.7850	0.7703
389.3440	0.7772
402.1790	0.7812
415.2920	0.7853
428.6880	0.7904
442.3680	0.7996
456.3360	0.8053
470.5960	0.8085
485.1500	0.8142

TABLE S35: Raw data for Ca as calculated with PBE in Castep.

V_{prim} (Å^3)	CFR fraction
4.0000	0.0000
4.6305	0.0000
5.3240	0.0000
6.0835	0.0000
6.9120	0.0000
7.8125	0.0000
8.7880	0.0000
9.8415	0.0000
10.9760	0.0000
12.1945	0.0000
13.5000	0.0000
14.8955	0.0000
16.3840	0.0000
17.9685	0.0000
19.6520	0.0000
21.4375	0.0000
23.3280	0.0000
25.3265	0.0000
27.4360	0.0000
29.6595	0.0000
32.0000	0.0000
34.4605	0.0000
37.0440	0.0000
39.7535	0.0000
42.5920	0.0000
45.5625	0.0000
48.6680	0.0000
51.9115	0.0000
55.2960	0.0000
58.8245	0.0000
62.5000	0.0000
66.3255	0.0000
70.3040	0.0000
74.4385	0.0000
78.7320	0.0000
83.1875	0.0000
87.8080	0.0000
92.5965	0.0000
97.5560	0.0000
102.6900	0.0000
108.0000	0.0000
113.4900	0.0000
119.1640	0.0000
125.0230	0.0000
131.0720	0.0000
137.3120	0.0000
143.7480	0.0000
150.3820	0.0032
157.2160	0.0683
164.2550	0.1777
171.5000	0.2383
178.9550	0.2798
186.6240	0.3148
194.5080	0.3443
202.6120	0.3760
210.9380	0.4071
219.4880	0.4406
228.2670	0.4711
237.2760	0.5008
⋮	⋮

V_{prim} (Å^3)	CFR fraction
⋮	⋮
246.5200	0.5208
256.0000	0.5415
265.7200	0.5598
275.6840	0.5734
285.8940	0.5889
296.3520	0.6042
307.0620	0.6192
318.0280	0.6352
329.2510	0.6467
340.7360	0.6605
352.4850	0.6721
364.5000	0.6840
376.7850	0.6948
389.3440	0.7056
402.1790	0.7151
415.2920	0.7242
428.6880	0.7330
442.3680	0.7432
456.3360	0.7499
470.5960	0.7589
485.1500	0.7653

TABLE S36: Raw data for Sr as calculated with PBE in Castep.

V_{prim} (Å^3)	CFR fraction
4.0000	0.0000
4.6305	0.0000
5.3240	0.0000
6.0835	0.0000
6.9120	0.0000
7.8125	0.0000
8.7880	0.0000
9.8415	0.0000
10.9760	0.0000
12.1945	0.0000
13.5000	0.0000
14.8955	0.0000
16.3840	0.0000
17.9685	0.0000
19.6520	0.0000
21.4375	0.0000
23.3280	0.0000
25.3265	0.0000
27.4360	0.0000
29.6595	0.0000
32.0000	0.0000
34.4605	0.0000
37.0440	0.0000
39.7535	0.0000
42.5920	0.0000
45.5625	0.0000
48.6680	0.0000
51.9115	0.0000
55.2960	0.0000
58.8245	0.0000
62.5000	0.0000
66.3255	0.0000
70.3040	0.0000
74.4385	0.0000
78.7320	0.0000
83.1875	0.0000
87.8080	0.0000
92.5965	0.0000
97.5560	0.0000
102.6900	0.0000
108.0000	0.0000
113.4900	0.0000
119.1640	0.0000
125.0230	0.0000
131.0720	0.0000
137.3120	0.0011
143.7480	0.0000
150.3820	0.0018
157.2160	0.0048
164.2550	0.0066
171.5000	0.0000
178.9550	0.0062
186.6240	0.0206
194.5080	0.0808
202.6120	0.1777
210.9380	0.2240
219.4880	0.2693
228.2670	0.3002
237.2760	0.3264
⋮	⋮
246.5200	0.3608
256.0000	0.3901
265.7200	0.4192
275.6840	0.4482
285.8940	0.4711
296.3520	0.4913
307.0620	0.5125
318.0280	0.5294
329.2510	0.5507
340.7360	0.5620
352.4850	0.5799
364.5000	0.5946
376.7850	0.6059
389.3440	0.6144
402.1790	0.6305
415.2920	0.6404
428.6880	0.6506
442.3680	0.6616
456.3360	0.6712
470.5960	0.6820
485.1500	0.6944

TABLE S37: Raw data for Ba as calculated with PBE in Castep.

V_{prim} (Å^3)	CFR fraction
4.0000	0.0000
4.6305	0.0000
5.3240	0.0000
6.0835	0.0000
6.9120	0.0000
7.8125	0.0000
8.7880	0.0000
9.8415	0.0000
10.9760	0.0000
12.1945	0.0000
13.5000	0.0000
14.8955	0.0000
16.3840	0.0000
17.9685	0.0000
19.6520	0.0000
21.4375	0.0000
23.3280	0.0000
25.3265	0.0000
27.4360	0.0000
29.6595	0.0000
32.0000	0.0000
34.4605	0.0000
37.0440	0.0000
39.7535	0.0000
42.5920	0.0000
45.5625	0.0000
48.6680	0.0000
51.9115	0.0000
55.2960	0.0000
58.8245	0.0000
62.5000	0.0000
66.3255	0.0000
70.3040	0.0000
74.4385	0.0000
78.7320	0.0000
83.1875	0.0000
87.8080	0.0000
92.5965	0.0000
97.5560	0.0000
102.6900	0.0000
108.0000	0.0000
113.4900	0.0000
119.1640	0.0000
125.0230	0.0000
131.0720	0.0000
137.3120	0.0000
143.7480	0.0000
150.3820	0.0000
157.2160	0.0000
164.2550	0.0000
171.5000	0.0000
178.9550	0.0000
186.6240	0.0003
194.5080	0.0000
202.6120	0.0000
210.9380	0.0039
219.4880	0.0078
228.2670	0.0108
237.2760	0.0446
⋮	⋮
246.5200	0.1016
256.0000	0.1691
265.7200	0.2206
275.6840	0.2636
285.8940	0.2989
296.3520	0.3304
307.0620	0.3591
318.0280	0.3852
329.2510	0.4142
340.7360	0.4424
352.4850	0.4714
364.5000	0.4992
376.7850	0.5192
389.3440	0.5400
402.1790	0.5546
415.2920	0.5706
428.6880	0.5844
442.3680	0.5989
456.3360	0.6108
470.5960	0.6220
485.1500	0.6377

TABLE S38: Raw data for Ra as calculated with PBE in Castep.

V_{prim} (Å^3)	CFR fraction
4.0000	0.0000
4.6305	0.0000
5.3240	0.0000
6.0835	0.0000
6.9120	0.0000
7.8125	0.0000
8.7880	0.0000
9.8415	0.0000
10.9760	0.0000
12.1945	0.0000
13.5000	0.0000
14.8955	0.0000
16.3840	0.0000
17.9685	0.0000
19.6520	0.0000
21.4375	0.0000
23.3280	0.0000
25.3265	0.0000
27.4360	0.0000
29.6595	0.0000
32.0000	0.0000
34.4605	0.0000
37.0440	0.0000
39.7535	0.0000
42.5920	0.0000
45.5625	0.0000
48.6680	0.0000
51.9115	0.0000
55.2960	0.0000
58.8245	0.0000
62.5000	0.0000
66.3255	0.0000
70.3040	0.0000
74.4385	0.0000
78.7320	0.0000
83.1875	0.0000
87.8080	0.0000
92.5965	0.0000
97.5560	0.0000
102.6900	0.0000
108.0000	0.0000
113.4900	0.0000
119.1640	0.0000
125.0230	0.0000
131.0720	0.0000
137.3120	0.0000
143.7480	0.0000
150.3820	0.0000
157.2160	0.0000
164.2550	0.0000
171.5000	0.0000
178.9550	0.0082
186.6240	0.0082
194.5080	0.0083
202.6120	0.0079
210.9380	0.0079
219.4880	0.0146
228.2670	0.0126
237.2760	0.0200
⋮	⋮

V_{prim} (Å^3)	CFR fraction
⋮	⋮
246.5200	0.0444
256.0000	0.1211
265.7200	0.1902
275.6840	0.2390
285.8940	0.2735
296.3520	0.3009
307.0620	0.3213
318.0280	0.3456
329.2510	0.3732
340.7360	0.3998
352.4850	0.4278
364.5000	0.4507
376.7850	0.4713
389.3440	0.4923
402.1790	0.5110
415.2920	0.5273
428.6880	0.5430
442.3680	0.5553
456.3360	0.5716
470.5960	0.5816
485.1500	0.5942

S4. RAW DATA FOR GROUP 14 ELEMENTAL SOLIDS

TABLE S39: Raw data for C as calculated with PBE in VASP.

V_{prim} (Å^3)	CFR fraction	Band gap from DOS (eV)
11.3748	0.0000	4.1395
13.3957	0.0000	3.7061
15.6427	0.0000	3.4592
18.1279	0.0000	3.0474
20.8634	0.0212	2.3060
23.8610	0.1116	0.5534
27.1328	0.1794	0.0000
30.6909	0.2407	0.0000
34.5471	0.3036	0.0000
38.7135	0.3615	0.0000
43.2022	0.4113	0.0000
48.0250	0.4548	0.0000
53.1940	0.4946	0.0000
58.7213	0.5302	0.0000
64.6187	0.5637	0.0000
70.8983	0.5943	0.0000
77.5722	0.6228	0.0000
84.6522	0.6492	0.0000
92.1505	0.6747	0.0000
100.0789	0.6986	0.0000
108.4495	0.7214	0.0000
117.2744	0.7436	0.0000
126.5654	0.7654	0.0000
136.3346	0.7839	0.0000
146.5941	0.7981	0.0000
157.3557	0.8104	0.0000
168.6315	0.8217	0.0000
180.4336	0.8321	0.0000
192.7738	0.8421	0.0000
205.6642	0.8509	0.0000
219.1169	0.8593	0.0000
233.1437	0.8669	0.0000
247.7567	0.8743	0.0000

TABLE S40: Raw data for Si as calculated with PBE in VASP.

V_{prim} (Å^3)	CFR fraction	Band gap from DOS (eV)
40.9168	0.0000	0.5507
45.5711	0.0000	0.7547
48.7857	0.0064	0.8074
50.5655	0.0242	0.7107
55.9121	0.0849	0.0000
61.6230	0.1457	0.0000
67.7100	0.1885	0.0000
74.1852	0.2351	0.0000
81.0607	0.2779	0.0000
88.3483	0.3186	0.0000
96.0601	0.3554	0.0000
104.2082	0.3890	0.0000
112.8044	0.4199	0.0000
121.8609	0.4493	0.0000
131.3895	0.4764	0.0000
141.4023	0.5022	0.0000
151.9114	0.5264	0.0000
162.9286	0.5491	0.0000
174.4660	0.5709	0.0000
186.5357	0.5916	0.0000
199.1495	0.6114	0.0000
212.3195	0.6304	0.0000
226.0578	0.6488	0.0000
240.3762	0.6661	0.0000
255.2868	0.6834	0.0000

TABLE S41: Raw data for C as calculated with LSDA in VASP.

V_{prim} (Å^3)	CFR fraction	Band gap from DOS (eV)
10.9967	0.0000	4.0588
12.9738	0.0000	3.7563
15.1746	0.0000	3.3818
17.6112	0.0000	3.0743
20.2957	0.0000	2.5228
23.2399	0.0097	1.0881
26.4560	0.0827	0.0000
29.9558	0.1643	0.0000
33.7514	0.2401	0.0000
37.8549	0.3093	0.0000
42.2781	0.3676	0.0000
47.0331	0.4171	0.0000
52.1320	0.4621	0.0000
57.5866	0.5012	0.0000
63.4090	0.5374	0.0000
69.6113	0.5703	0.0000
76.2053	0.6005	0.0000
83.2031	0.6294	0.0000
90.6168	0.6555	0.0000
98.4582	0.6803	0.0000
106.7394	0.7041	0.0000
115.4725	0.7258	0.0000
124.6693	0.7471	0.0000
134.3419	0.7665	0.0000
144.5024	0.7837	0.0000
155.1626	0.7981	0.0000
166.3347	0.8106	0.0000
178.0305	0.8224	0.0000
190.2621	0.8327	0.0000
203.0416	0.8422	0.0000
216.3808	0.8512	0.0000
230.2918	0.8591	0.0000
244.7867	0.8666	0.0000

TABLE S42: Raw data for Si as calculated with LSDA in VASP.

V_{prim} (Å^3)	CFR fraction	Band gap from DOS (eV)
39.3660	0.0000	0.3872
43.9040	0.0000	0.6069
48.7780	0.0000	0.6498
54.0000	0.0105	0.1719
59.5820	0.0497	0.0000
65.5360	0.1094	0.0000
71.8740	0.1685	0.0000
78.6080	0.2202	0.0000
85.7500	0.2672	0.0000
93.3120	0.3090	0.0000
101.3060	0.3468	0.0000
109.7440	0.3819	0.0000
118.6380	0.4135	0.0000
128.0000	0.4430	0.0000
137.8420	0.4716	0.0000
148.1760	0.4970	0.0000
159.0140	0.5221	0.0000
170.3680	0.5455	0.0000
182.2500	0.5678	0.0000
194.6720	0.5892	0.0000
207.6460	0.6091	0.0000
221.1840	0.6285	0.0000
235.2980	0.6472	0.0000
250.0000	0.6648	0.0000

TABLE S43: Raw data for C as calculated with PBE in Castep.

V_{prim} (Å^3)	CFR fraction
3.9062	0.0000
4.3940	0.0000
4.9208	0.0000
5.4880	0.0000
6.0972	0.0000
6.7500	0.0000
7.4478	0.0000
8.1920	0.0000
8.9842	0.0000
9.8260	0.0000
10.7188	0.0000
11.6640	0.0000
12.6633	0.0000
13.7180	0.0000
14.8297	0.0000
16.0000	0.0000
17.2302	0.0000
18.5220	0.0000
19.8767	0.0000
21.2960	0.0015
22.7812	0.0270
24.3340	0.0986
25.9558	0.1420
27.6480	0.1723
29.4122	0.2062
31.2500	0.2465
33.1628	0.2781
35.1520	0.3125
37.2192	0.3388
39.3660	0.3700
41.5938	0.3923
43.9040	0.4157
46.2982	0.4402
48.7780	0.4602
51.3448	0.4800
54.0000	0.4969
56.7452	0.5169
59.5820	0.5373
62.5118	0.5536
65.5360	0.5724
68.6562	0.5900
71.8740	0.6077
75.1908	0.6258
78.6080	0.6447
82.1272	0.6581
85.7500	0.6731
89.4778	0.6911
93.3120	0.7033
97.2542	0.7137
101.3060	0.7253
105.4688	0.7362
109.7440	0.7474
114.1332	0.7576
118.6380	0.7664
123.2598	0.7776
128.0000	0.7847
132.8602	0.7922
137.8420	0.8000
142.9468	0.8063
⋮	⋮
148.1760	0.8136
153.5312	0.8200
159.0140	0.8269
164.6258	0.8328
170.3680	0.8385
176.2422	0.8441
182.2500	0.8501
188.3928	0.8550
194.6720	0.8603
201.0900	0.8652
207.6460	0.8687
214.3440	0.8731
221.1840	0.8765
228.1680	0.8807
235.2980	0.8844
242.5740	0.8878

TABLE S44: Raw data for Si as calculated with PBE in Castep.

V_{prim} (Å^3)	CFR fraction
3.9062	0.0000
4.3940	0.0000
4.9208	0.0000
5.4880	0.0000
6.0972	0.0000
6.7500	0.0000
7.4478	0.0000
8.1920	0.0000
8.9842	0.0000
9.8260	0.0000
10.7188	0.0000
11.6640	0.0000
12.6633	0.0000
13.7180	0.0000
14.8297	0.0000
16.0000	0.0000
17.2302	0.0000
18.5220	0.0000
19.8767	0.0000
21.2960	0.0000
22.7812	0.0000
24.3340	0.0000
25.9558	0.0000
27.6480	0.0000
29.4122	0.0000
31.2500	0.0000
33.1628	0.0000
35.1520	0.0000
37.2192	0.0000
39.3660	0.0000
41.5938	0.0000
43.9040	0.0095
46.2982	0.0020
48.7780	0.0093
51.3448	0.0176
54.0000	0.0208
56.7452	0.0614
59.5820	0.1012
62.5118	0.1289
65.5360	0.1677
68.6562	0.1903
71.8740	0.2162
75.1908	0.2368
78.6080	0.2632
82.1272	0.2843
85.7500	0.2955
89.4778	0.3277
93.3120	0.3444
97.2542	0.3609
101.3060	0.3779
105.4688	0.3959
109.7440	0.4042
114.1332	0.4236
118.6380	0.4381
123.2598	0.4504
128.0000	0.4648
132.8602	0.4792
137.8420	0.4887
142.9468	0.5017
⋮	⋮

V_{prim} (Å^3)	CFR fraction
⋮	⋮
148.1760	0.5154
153.5312	0.5292
159.0140	0.5456
164.6258	0.5569
170.3680	0.5639
176.2422	0.5773
182.2500	0.5851
188.3928	0.5964
194.6720	0.6056
201.0900	0.6121
207.6460	0.6224
214.3440	0.6357
221.1840	0.6455
228.1680	0.6540
235.2980	0.6659
242.5740	0.6758

TABLE S45: Raw data for Ge as calculated with PBE in Castep.

V_{prim} (Å^3)	CFR fraction
3.9062	0.0000
4.3940	0.0000
4.9207	0.0000
5.4880	0.0000
6.0972	0.0000
6.7500	0.0000
7.4478	0.0000
8.1920	0.0000
8.9842	0.0000
9.8260	0.0000
10.7188	0.0000
11.6640	0.0000
12.6633	0.0000
13.7180	0.0000
14.8297	0.0000
16.0000	0.0000
17.2302	0.0000
18.5220	0.0000
19.8767	0.0000
21.2960	0.0000
22.7812	0.0000
24.3340	0.0000
25.9558	0.0000
27.6480	0.0000
29.4123	0.0000
31.2500	0.0000
33.1627	0.0000
35.1520	0.0000
37.2192	0.0000
39.3660	0.0000
41.5938	0.0000
43.9040	0.0000
46.2983	0.0000
48.7780	0.0000
51.3448	0.0008
54.0000	0.0065
56.7452	0.0284
59.5820	0.0616
62.5117	0.1063
65.5360	0.1401
68.6562	0.1633
71.8740	0.1882
75.1908	0.2109
78.6080	0.2322
82.1273	0.2523
85.7500	0.2727
89.4777	0.2919
93.3120	0.3104
97.2542	0.3287
101.3060	0.3456
105.4690	0.3628
109.7440	0.3789
114.1330	0.3934
118.6380	0.4087
123.2600	0.4239
128.0000	0.4382

TABLE S46: Raw data for Sn as calculated with PBE in Castep.

V_{prim} (Å^3)	CFR fraction
3.9062	0.0000
4.3940	0.0000
4.9207	0.0000
5.4880	0.0000
6.0972	0.0000
6.7500	0.0000
7.4478	0.0000
8.1920	0.0000
8.9842	0.0000
9.8260	0.0000
10.7188	0.0000
11.6640	0.0000
12.6633	0.0000
13.7180	0.0000
14.8297	0.0000
16.0000	0.0000
17.2302	0.0000
18.5220	0.0000
19.8767	0.0000
21.2960	0.0000
22.7812	0.0000
24.3340	0.0000
25.9558	0.0000
27.6480	0.0000
29.4123	0.0000
31.2500	0.0000
33.1627	0.0000
35.1520	0.0000
37.2192	0.0000
39.3660	0.0000
41.5938	0.0000
43.9040	0.0000
46.2983	0.0000
48.7780	0.0000
51.3448	0.0000
54.0000	0.0000
56.7452	0.0000
59.5820	0.0000
62.5117	0.0000
65.5360	0.0001
68.6562	0.0027
71.8740	0.0136
75.1908	0.0349
78.6080	0.0655
82.1273	0.1074
85.7500	0.1375
89.4777	0.1621
93.3120	0.1850
97.2542	0.2056
101.3060	0.2252
105.4690	0.2434
109.7440	0.2641
114.1330	0.2831
118.6380	0.3009
123.2600	0.3178
128.0000	0.3343
132.8600	0.3485
137.8420	0.3651
142.9470	0.3798
⋮	⋮
148.1760	0.3915
153.5310	0.4071
159.0140	0.4202
164.6260	0.4338
170.3680	0.4454
176.2420	0.4589
182.2500	0.4712
188.3930	0.4836
194.6720	0.4918
201.0890	0.5040
207.6460	0.5147
214.3440	0.5223
221.1840	0.5329
228.1680	0.5428
235.2980	0.5539
242.5750	0.5631

TABLE S47: Raw data for Pb as calculated with PBE in Castep.

V_{prim} (Å^3)	CFR fraction
3.9062	0.0000
4.3940	0.0000
4.9207	0.0000
5.4880	0.0000
6.0972	0.0000
6.7500	0.0000
7.4478	0.0000
8.1920	0.0000
8.9842	0.0000
9.8260	0.0000
10.7188	0.0000
11.6640	0.0000
12.6633	0.0000
13.7180	0.0000
14.8297	0.0000
16.0000	0.0000
17.2302	0.0000
18.5220	0.0000
19.8767	0.0000
21.2960	0.0000
22.7812	0.0000
24.3340	0.0000
25.9558	0.0000
27.6480	0.0000
29.4123	0.0000
31.2500	0.0000
33.1627	0.0000
35.1520	0.0000
37.2192	0.0000
39.3660	0.0000
41.5938	0.0000
43.9040	0.0000
46.2983	0.0000
48.7780	0.0000
51.3448	0.0000
54.0000	0.0000
56.7452	0.0000
59.5820	0.0000
62.5117	0.0000
65.5360	0.0000
68.6562	0.0000
71.8740	0.0000
75.1908	0.0023
78.6080	0.0177
82.1273	0.0418
85.7500	0.0711
89.4777	0.1127
93.3120	0.1429
97.2542	0.1641
101.3060	0.1877
105.4690	0.2061
109.7440	0.2239
114.1330	0.2426
118.6380	0.2628
123.2600	0.2771
128.0000	0.2971
132.8600	0.3106
137.8420	0.3295
142.9470	0.3429
⋮	⋮

V_{prim} (Å^3)	CFR fraction
⋮	⋮
148.1760	0.3584
153.5310	0.3726
159.0140	0.3866
164.6260	0.3977
170.3680	0.4124
176.2420	0.4230
182.2500	0.4369
188.3930	0.4481
194.6720	0.4612
201.0890	0.4706
207.6460	0.4838
214.3440	0.4911
221.1840	0.5033
228.1680	0.5128
235.2980	0.5225
242.5750	0.5328

S5. RAW DATA FOR GROUP 18 ELEMENTAL SOLIDS

TABLE S48: Raw data for Ne as calculated with PBE in VASP.

V_{prim} (Å^3)	CFR fraction	Band gap from DOS (eV)
5.7873	0.0933	18.5758
6.0972	0.1847	17.9035
6.4181	0.3122	17.5081
6.7500	0.3719	16.9491
8.1920	0.5404	14.9407
9.8260	0.6535	13.8288
11.6640	0.7240	12.9718
13.7180	0.7763	12.4658
16.0000	0.8088	12.1625
18.5220	0.8356	11.7600
21.2960	0.8570	11.5588
24.3340	0.8745	11.4974
27.6480	0.8899	11.2233
31.2500	0.9024	11.2782
35.1520	0.9131	11.2431
39.3660	0.9227	11.3382
43.9040	0.9306	11.3177
48.7780	0.9373	11.3249
54.0000	0.9436	11.3459

TABLE S49: Raw data for Ne as calculated with LSDA in VASP.

V_{prim} (Å^3)	CFR fraction	Band gap from DOS (eV)
5.7873	0.0261	18.3436
6.0972	0.0576	17.6710
6.4181	0.1407	17.0007
6.7500	0.2294	16.4522
8.1920	0.5164	14.4664
9.8260	0.6455	13.4261
11.6640	0.7178	12.4733
13.7180	0.7691	11.9869
16.0000	0.8060	11.6004
18.5220	0.8354	11.3754
21.2960	0.8570	11.3931
24.3340	0.8745	11.3476
27.6480	0.8899	11.2333
31.2500	0.9024	11.3534
35.1520	0.9131	11.3287
39.3660	0.9227	11.4308
43.9040	0.9306	11.5933
48.7780	0.9373	11.6459
54.0000	0.9436	11.7969

TABLE S50: Raw data for He as calculated with PBE in Castep.

V_{prim} (Å^3)	CFR fraction
0.2500	0.0000
0.3327	0.0000
0.4320	0.0000
0.5493	0.0000
0.6860	0.0000
0.8438	0.0000
1.0240	0.0000
1.2283	0.0000
1.4580	0.0000
1.7147	0.0000
2.0000	0.0000
2.3152	0.0000
2.6620	0.0365
3.0417	0.2798
3.4560	0.4887
3.9062	0.6073
4.3940	0.6560
4.9207	0.7319
5.4880	0.7805
6.0972	0.8058
6.7500	0.8310
7.4478	0.8523
8.1920	0.8745
8.9842	0.8871
9.8260	0.8966
10.7188	0.9104
11.6640	0.9145
12.6633	0.9207
13.7180	0.9315
14.8297	0.9356
16.0000	0.9407
17.2302	0.9441
18.5220	0.9501
19.8767	0.9534
21.2960	0.9556
22.7812	0.9585
24.3340	0.9615
25.9558	0.9636
27.6480	0.9665
29.4123	0.9694
31.2500	0.9711
33.1627	0.9728
35.1520	0.9733
37.2192	0.9760
39.3660	0.9764
41.5938	0.9773
43.9040	0.9797
46.2983	0.9809
48.7780	0.9812
51.3448	0.9824
54.0000	0.9829
56.7452	0.9834
59.5820	0.9843
62.5117	0.9852
65.5360	0.9863
68.6562	0.9863
71.8740	0.9871
75.1908	0.9878
78.6080	0.9885
⋮	⋮
82.1273	0.9887
85.7500	0.9891
89.4777	0.9898
93.3120	0.9901
97.2542	0.9904
101.3060	0.9909
105.4690	0.9914
109.7440	0.9920
114.1330	0.9921
118.6380	0.9921
123.2600	0.9926
128.0000	0.9928

TABLE S51: Raw data for Ne as calculated with PBE in Castep.

V_{prim} (Å^3)	CFR fraction
3.9062	0.0000
4.3940	0.0000
4.9207	0.0000
5.4880	0.0359
6.0972	0.1041
6.7500	0.2904
7.4478	0.4156
8.1920	0.4829
8.9842	0.5534
9.8260	0.6158
10.7188	0.6594
11.6640	0.6909
12.6633	0.7259
13.7180	0.7556
14.8297	0.7745
16.0000	0.7939
17.2302	0.8111
18.5220	0.8253
19.8767	0.8388
21.2960	0.8494
22.7812	0.8594
24.3340	0.8702
25.9558	0.8772
27.6480	0.8868
29.4123	0.8949
31.2500	0.9007
33.1627	0.9049
35.1520	0.9111
37.2192	0.9157
39.3660	0.9197
41.5938	0.9249
43.9040	0.9280
46.2983	0.9307
48.7780	0.9364
51.3448	0.9396
54.0000	0.9422
56.7452	0.9436
59.5820	0.9470
62.5117	0.9497
65.5360	0.9525
68.6562	0.9535
71.8740	0.9565
75.1908	0.9583
78.6080	0.9599
82.1273	0.9621
85.7500	0.9634
89.4777	0.9650
93.3120	0.9661
97.2542	0.9682
101.3060	0.9694
105.4690	0.9704
109.7440	0.9725
118.6380	0.9737
123.2600	0.9746
128.0000	0.9755
132.8600	0.9762
137.8420	0.9773
142.9470	0.9785
148.1760	0.9787
⋮	⋮

V_{prim} (Å^3)	CFR fraction
⋮	⋮
153.5310	0.9795
159.0140	0.9802
164.6260	0.9812

TABLE S52: Raw data for Ar as calculated with PBE in Castep.

V_{prim} (Å^3)	CFR fraction
3.9062	0.0000
4.3940	0.0000
4.9207	0.0000
5.4880	0.0000
6.0972	0.0000
6.7500	0.0000
7.4478	0.0000
8.1920	0.0000
8.9842	0.0000
9.8260	0.0000
10.7188	0.0000
11.6640	0.0000
12.6633	0.0000
13.7180	0.0004
14.8297	0.0346
16.0000	0.0745
17.2302	0.1886
18.5220	0.3148
19.8767	0.4153
21.2960	0.4775
22.7812	0.5201
24.3340	0.5577
25.9558	0.6075
27.6480	0.6405
29.4123	0.6620
31.2500	0.6832
33.1627	0.7079
35.1520	0.7326
37.2192	0.7475
39.3660	0.7626
41.5938	0.7791
43.9040	0.7936
46.2983	0.8051
48.7780	0.8159
51.3448	0.8249
54.0000	0.8374
56.7452	0.8412
59.5820	0.8505
62.5117	0.8583
65.5360	0.8652
68.6562	0.8705
71.8740	0.8771
75.1908	0.8816
78.6080	0.8874
82.1273	0.8935
85.7500	0.8955
89.4777	0.9016
93.3120	0.9068
97.2542	0.9090
101.3060	0.9127
105.4690	0.9175
109.7440	0.9195
114.1330	0.9244
118.6380	0.9252
123.2600	0.9288
128.0000	0.9309

TABLE S53: Raw data for Kr as calculated with PBE in Castep.

V_{prim} (Å^3)	CFR fraction
3.9062	0.0000
4.3940	0.0000
4.9207	0.0000
5.4880	0.0000
6.0972	0.0000
6.7500	0.0000
7.4478	0.0000
8.1920	0.0000
8.9842	0.0000
9.8260	0.0000
10.7188	0.0000
11.6640	0.0000
12.6633	0.0000
13.7180	0.0000
14.8297	0.0000
16.0000	0.0000
17.2302	0.0000
18.5220	0.0000
19.8767	0.0140
21.2960	0.0396
22.7812	0.0852
24.3340	0.1839
25.9558	0.2970
27.6480	0.3921
29.4123	0.4530
31.2500	0.5050
33.1627	0.5314
35.1520	0.5740
37.2192	0.6097
39.3660	0.6343
41.5938	0.6668
43.9040	0.6832
46.2983	0.7079
48.7780	0.7229
51.3448	0.7394
54.0000	0.7556
56.7452	0.7661
59.5820	0.7796
62.5117	0.7901
65.5360	0.8006
68.6562	0.8087
71.8740	0.8187
75.1908	0.8276
78.6080	0.8347
82.1273	0.8416
85.7500	0.8500
89.4777	0.8562
93.3120	0.8617
97.2542	0.8646
101.3060	0.8756
105.4690	0.8772
109.7440	0.8828
114.1330	0.8892
118.6380	0.8915
123.2600	0.8964
128.0000	0.9006

TABLE S54: Raw data for Xe as calculated with PBE in Castep.

V_{prim} (Å^3)	CFR fraction
4.3940	0.0000
4.9207	0.0000
5.4880	0.0000
6.0972	0.0000
6.7500	0.0000
7.4478	0.0000
8.1920	0.0000
8.9842	0.0000
9.8260	0.0000
10.7188	0.0000
11.6640	0.0000
12.6633	0.0000
13.7180	0.0000
14.8297	0.0000
16.0000	0.0000
17.2302	0.0000
18.5220	0.0000
19.8767	0.0000
21.2960	0.0000
22.7812	0.0000
24.3340	0.0000
25.9558	0.0003
27.6480	0.0003
29.4123	0.0177
31.2500	0.0200
33.1627	0.0796
35.1520	0.1097
37.2192	0.2275
39.3660	0.3067
41.5938	0.3767
43.9040	0.4407
46.2983	0.4856
48.7780	0.5124
51.3448	0.5530
54.0000	0.5850
56.7452	0.6147
59.5820	0.6271
62.5117	0.6556
65.5360	0.6769
68.6562	0.6884
71.8740	0.7074
75.1908	0.7250
78.6080	0.7426
82.1273	0.7550
85.7500	0.7599
89.4777	0.7708
93.3120	0.7832
97.2542	0.7924
101.3060	0.7986
105.4690	0.8110
109.7440	0.8192
114.1330	0.8245
118.6380	0.8341
123.2600	0.8389
128.0000	0.8427